




**COMMUNICATION**

# DEG/ENaC/ASIC channels vary in their sensitivity to anti-hypertensive and non-steroidal anti-inflammatory drugs

Sylvia Fechner<sup>1</sup> , Isabel D'Alessandro<sup>1</sup>, Lingxin Wang<sup>1</sup>, Calvin Tower<sup>1</sup> , Li Tao<sup>2</sup>, and Miriam B. Goodman<sup>1</sup> 

The degenerin channels, epithelial sodium channels, and acid-sensing ion channels (DEG/ENaC/ASICs) play important roles in sensing mechanical stimuli, regulating salt homeostasis, and responding to acidification in the nervous system. They have two transmembrane domains separated by a large extracellular domain and are believed to assemble as homomeric or heteromeric trimers. Based on studies of selected family members, these channels are assumed to form nonvoltage-gated and sodium-selective channels sensitive to the anti-hypertensive drug amiloride. They are also emerging as a target of nonsteroidal anti-inflammatory drugs (NSAIDs). *Caenorhabditis elegans* has more than two dozen genes encoding DEG/ENaC/ASIC subunits, providing an excellent opportunity to examine variations in drug sensitivity. Here, we analyze a subset of the *C. elegans* DEG/ENaC/ASIC proteins to test the hypothesis that individual family members vary not only in their ability to form homomeric channels but also in their drug sensitivity. We selected a panel of *C. elegans* DEG/ENaC/ASICs that are coexpressed in mechanosensory neurons and expressed gain-of-function or *d* mutants in *Xenopus laevis* oocytes. We found that only DEGT-1d, UNC-8d, and MEC-4d formed homomeric channels and that, unlike MEC-4d and UNC-8d, DEGT-1d channels were insensitive to amiloride and its analogues. As reported for rat ASIC1a, NSAIDs inhibit DEGT-1d and UNC-8d channels. Unexpectedly, MEC-4d was strongly potentiated by NSAIDs, an effect that was decreased by mutations in the putative NSAID-binding site in the extracellular domain. Collectively, these findings reveal that not all DEG/ENaC/ASIC channels are amiloride-sensitive and that NSAIDs can both inhibit and potentiate these channels.

## Introduction

The degenerin, epithelial sodium, and acid-sensing ion channels (DEG/ENaC/ASICs) are present in most if not all metazoan genomes and expressed in diverse tissues, including the epithelia of several organs and in the central and peripheral nervous systems (Eastwood and Goodman, 2012; Kellenberger and Schild, 2002). At least two DEG proteins are known to be mechanosensitive, ENaCs are constitutively active and can be regulated by shear stress, and ASICs are activated by proton binding (Eastwood and Goodman, 2012). The DEGs were identified in *Caenorhabditis elegans* by virtue of their role in mechanosensation and by gain-of-function mutations that cause neuronal degeneration (Chalfie and Wolinsky, 1990; Driscoll and Chalfie, 1991; Huang and Chalfie, 1994). The ENaCs were identified via expression of rodent capped RNAs (cRNAs) in *Xenopus laevis* oocytes followed by functional screening (Canessa et al., 1995). The proteins that form ASICs were based on their homology to DEGs and ENaCs (García-Añoveros et al., 1997; Kellenberger and Schild, 2002; Waldmann et al., 1997).

All of these proteins have short intracellular amino and carboxy termini and two transmembrane domains linked by a large extracellular domain that is divided into structures described by a hand holding a ball: wrist, finger, ball, and knuckle. This view has emerged from high-resolution structures derived from x-ray diffraction of protein crystals (Baconguis et al., 2014; Dawson et al., 2012; Gonzales et al., 2009; Jasti et al., 2007; Noreng et al., 2018) and cryo-electron microscopy of chicken ASIC1a (Sun et al., 2018; Yoder et al., 2018) and human ENaC (Noreng et al., 2018). Individual proteins assemble into trimers and form a pore along a common threefold axis at the center of the complex. The extracellular finger domain exhibits more sequence variation than other domains and the general topology of all family members is assumed to share the same fold as ASIC1a. Although ENaCs are formed from three distinct proteins, many DEGs and ASICs can form both homomeric and heteromeric channels. Thus, the ensemble of functional channels is expanded not only by genetic variation of individual

<sup>1</sup>Department of Molecular and Cellular Physiology, Stanford University, Stanford, CA; <sup>2</sup>Department of Biology, Stanford University, Stanford, CA.

Correspondence to M.B. Goodman: [mbgoodman@stanford.edu](mailto:mbgoodman@stanford.edu); S. Fechner: [sfechner@stanford.edu](mailto:sfechner@stanford.edu).

© 2021 Fechner et al. This article is distributed under the terms of an Attribution–Noncommercial–Share Alike–No Mirror Sites license for the first six months after the publication date (see <http://www.rupress.org/terms/>). After six months it is available under a Creative Commons License (Attribution–Noncommercial–Share Alike 4.0 International license, as described at <https://creativecommons.org/licenses/by-nc-sa/4.0/>).

channel subunits but also by the formation of heteromeric channels.

The ENaC channels are crucial for salt homeostasis and are blocked by amiloride (Garty and Benos, 1988; Palmer, 1992), a classic anti-hypertension drug that functions as an open-channel blocker (Schild et al., 1997). Sensitivity to amiloride and its analogues is not limited to mammalian family members or to ENaCs, however, but is also seen in DEG/ENaC/ASIC channels expressed in invertebrates. Amiloride is a potent (submicromolar half-maximal inhibitory concentration [ $IC_{50}$ ]) blocker of DEG and ENaC channels, but is at least 100-fold less potent as a blocker of ASIC channels (Canessa et al., 1994; Goodman et al., 2002; Vullo and Kellenberger, 2019). Despite widespread findings of amiloride as an inhibitor, amiloride is also reported to potentiate the activity of two DEG/ENaC/ASIC channels (Adams et al., 1999; Elkhatib et al., 2019). It is not known whether amiloride inhibition and potentiation arise from binding to similar or distinct sites. Among channels inhibited by amiloride, variations in sensitivity could reflect differences in binding affinity or in the efficacy of inhibition. It remains unknown whether or not sensitivity to amiloride or its analogues is a universal feature of DEG/ENaC/ASIC channels.

The ASIC channels are implicated in neurological disease and in pain sensation, but there are no potent and selective small molecule inhibitors of ASICs available (Boscardin et al., 2016; Hanukoglu and Hanukoglu, 2016; Kellenberger and Schild, 2015; Vullo and Kellenberger, 2019). Evidence is emerging that ASICs are targets of nonsteroidal anti-inflammatory drugs (NSAIDs). In particular, ibuprofen is an effective (micromolar  $IC_{50}$ ) allosteric inhibitor of H<sup>+</sup>-evoked ASIC1a currents, and mutations in the wrist and the first transmembrane domain reduce the apparent affinity for ibuprofen (Lynagh et al., 2017). This finding implicates NSAIDs as an additional class of small molecules affecting the function of DEG/ENaC/ASIC channels.

Whereas mammalian genomes have nine genes encoding ENaC and ASIC proteins (Hanukoglu and Hanukoglu, 2016; Kellenberger and Schild, 2002), the *C. elegans* genome harbors more than two dozen genes encoding DEG/ENaC/ASIC proteins (Goodman and Schwarz, 2003; Hobert, 2013). Thus, the *C. elegans* set of DEG/ENaC/ASIC proteins offers an excellent opportunity to examine variations in the biophysical properties within this superfamily. As an entry point for exploration, we expressed five DEG/ENaC/ASIC proteins in *Xenopus* oocytes individually, tested their ability to form functional channels, and examined their response to amiloride and its analogues as well as a set of NSAIDs. The five DEG/ENaC/ASIC proteins we studied, DEGT-1, DEL-1, UNC-8, MEC-10, and MEC-4, are expressed in touch receptor neurons (MEC-4, MEC-10, and DEGT-1; Driscoll and Chalfie, 1991; Huang and Chalfie, 1994; Chatzigeorgiou et al., 2010), mechanical nociceptors (UNC-8, MEC-10, and DEL-1; Tavernarakis et al., 1997; Chatzigeorgiou et al., 2010), and motor neurons (UNC-8 and DEL-1; Tavernarakis et al., 1997). All five proteins are either known or proposed to contribute to the formation of mechanosensitive ion channels (O'Hagan et al., 2005; Chatzigeorgiou et al., 2010; Tao et al., 2019; Liu et al., 2020). We used constitutively active gain-of-function or *d* mutant channel isoforms throughout the study.

Here, we found that DEL-1d fails to generate any detectable current on its own and confirmed prior work showing that MEC-10d (Goodman et al., 2002) is also not sufficient to generate current. By contrast, DEGT-1d forms a homomeric channel that is insensitive to amiloride and its analogues, has a more negative reversal potential than other channels, and is blocked by NSAIDs. Both MEC-4d and UNC-8d formed channels blocked by amiloride and carried currents, consistent with prior work (Goodman et al., 2002; Wang et al., 2013). Unexpectedly, MEC-4d current was strongly potentiated by NSAIDs, and sensitivity to these drugs was decreased by mutations in the extracellular domain that affect inhibition of ASIC1a by ibuprofen, a frontline NSAID drug. Collectively, these findings reveal that not all DEG/ENaC/ASIC channels are amiloride-sensitive and that NSAIDs can both potentiate and inhibit these channels.

## Materials and methods

### Expression constructs and molecular biology

Plasmids carrying native cDNAs encoding MEC-4, MEC-10, and other *C. elegans* DEG/ENaC/ASIC proteins derived from the *C. elegans* genome are subject to deletions and recombination when propagated in standard bacterial strains (Goodman et al., 2002; Chalfie et al., 2003). Previously, we circumvented this outcome using SMC4, a bacterial strain specifically derived for this purpose (Goodman et al., 2002; Chalfie et al., 2003). Here, we used an alternative strategy that enables the propagation of expression plasmids in standard bacterial strains (5- $\alpha$  Competent *E. coli*, High Efficiency; NEB): synthetic cDNAs codon-optimized for expression in insect cells. Accordingly, we obtained plasmids containing synthesized codon-optimized cDNAs encoding full-length MEC-4, MEC-10, and DEGT-1 (GenScript) in the pGEM-HE oocyte expression vector (Liman et al., 1992). DEL-1 was codon-optimized for expression in *C. elegans* (IDT) based on the predicted sequence reported in wormbase release WS250. The predicted isoforms encoded by the *del-1* locus have been modified in a more recent database releases (WS274), and these changes are evident only in the amino-terminal domains. WS274 predicts three isoforms, and the isoform we used from WS250 encodes 18 amino acids that are not represented in the updated predictions. Unlike MEC-4, MEC-10, DEL-1, and DEGT-1, the UNC-8 isoform was not codon-optimized. This plasmid was obtained from L. Bianchi (University of Miami, Miami, FL), was used in prior studies (Matthewman et al., 2018, 2016; Miller-Fleming et al., 2016; Wang et al., 2013), and encodes the shortest of four predicted splice variants (R13A1.4d).

We studied the expressed channels as constitutively active or *degeneration* isoforms based on gain-of-function mutations identified in forward genetic screens or engineered into homologous residues. Because coexpressing MEC-2 yields larger currents than expressing MEC-4d alone and coexpressing MEC-2 with UNC-8d is either indifferent or may yield to larger currents than expressing UNC-8d alone (Brown et al., 2007; Goodman et al., 2002; Matthewman et al., 2016), we coexpressed MEC-2 with all DEG/ENaC/ASIC channels studied here.

We used *in vitro* mutagenesis (Q-5 Site-directed Mutagenesis Kit; NEB) to introduce the mutations creating *d* isoforms using

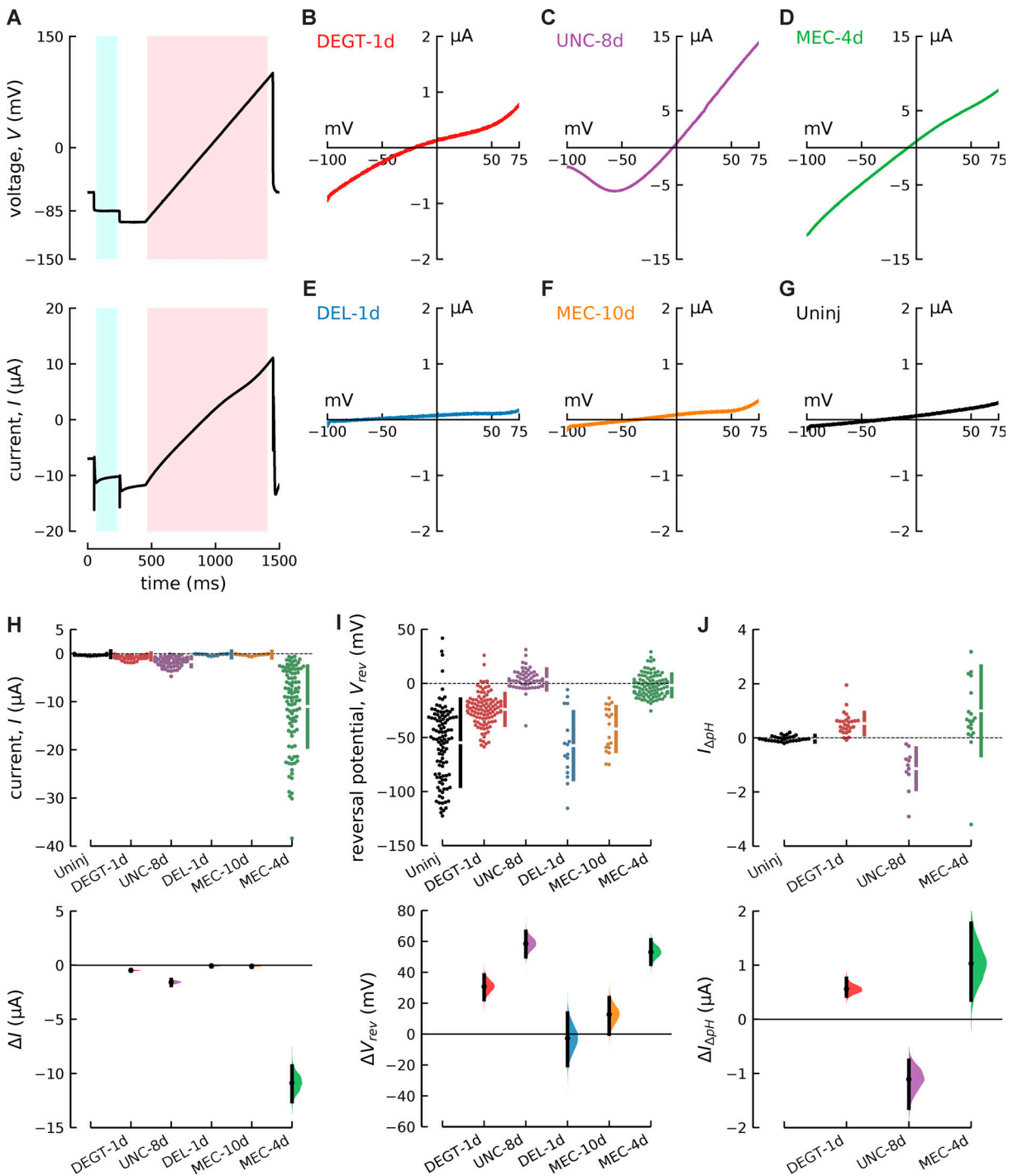


**Figure 1. The DEG/ENaC/ASIC subunits DEGT-1d, UNC-8d, and MEC-4d form homomeric channels in *Xenopus* oocytes, while DEL-1d and MEC-10d likely do not.** (A) Graphical representation of the voltage-clamp protocol (top) and total current measured in an oocyte expressing MEC-4d (bottom). Shaded areas are epochs at a holding potential of -85 mV (aqua) and a voltage ramp from -100 to 100 mV (pink) used to measure current amplitude and reversal potential, respectively. (B–G) Current–voltage curves measured in oocytes coexpressing MEC-2 and DEGT-1d (B), UNC-8d (C), MEC-4d (D), DEL-1d (E), MEC-10d (F), and uninjected (Uninj) oocytes (G). (H) Total current,  $I$  (at -85 mV) as a function of uninjected and expressed proteins (top) and estimation plot (bottom) showing the effect of channel protein expression relative to uninjected oocytes ( $\Delta I$ ). (I) Reversal potential ( $V_{rev}$ ) as a function of uninjected and expressed proteins (top) and estimation plot (bottom) showing the effect of channel protein expression relative to uninjected oocytes ( $\Delta V_{rev}$ ). Mean values, 95% confidence intervals, and statistical tests for the data in B–I are in Table 1. (J) Change in current (at -85 mV) induced by a pH shift from 8.4 to 6.4 ( $I_{\Delta pH}$ ) in uninjected oocytes and oocytes expressing DEGT-1d, UNC-8d, and MEC-4d (top), and estimation plot (bottom) showing the effect size relative to uninjected oocytes ( $\Delta I_{\Delta pH}$ ). Mean values, 95% confidence interval (in  $\mu$ A), and the two-sided P value of the Mann–Whitney test for J are as follows: DEGT-1d: 0.56  $\mu$ A (0.43–0.76),  $P = 4.70E-09$  ( $n = 27$ ); UNC-8d: -1.11  $\mu$ A (-1.64 to -0.76),  $P = 4.99E-07$  ( $n = 11$ ); and MEC-4d: 1.03  $\mu$ A (0.–1.78),  $P = 4.14E-06$  ( $n = 20$ ).

the following primers. All mutations were introduced into plasmids encoding wild-type protein, except for the mutants affecting the extracellular domain in MEC-4, which were introduced into plasmids encoding MEC-4(A713T) or MEC-4d. The primers used for mutagenesis are as follows: MEC-4(A713T), 5'-CTCTTGACTGACTTCGGTGG-3', 5'-GTTCCACGAAACCGTAGGCTT-3'; MEC-10(A676V), 5'-AAGATGATGGTTGACTTCGGC-3', 5'-CACGATACCGTAGGCCTC-3'; DEGT-1(A813T), 5'-CTCTTGACTGAGATCGGAGG-3', 5'-CAGGAACAAGTTGTAGGAGC-3'; UNC-8(G347E), 5'-AAAGATGCGGAAGCCATCACA-3', 5'-GAGGTCGCTCAATCCAAAAG-3'; DEL-1(A603V), 5'-AATTTGATGGTCGATATGGGAG-3', 5'-GAACCATGAATATGACTCG-3'; MEC-4(A713T, E704K), 5'-GGCCTACGGTTTCGTGAACCTCT-3', 5'-TTGGACTCGGTGAGCATCTCGAA-3'; MEC-4(A713T, E704A), 5'-GCGGACTCGGTGAGCATCTC-3', 5'-AGCCTACGGTTTCGTGAACCTC-3'.

### RNA preparation, validation, and oocyte injection

For each channel isoform, we generated cRNAs using *in vitro* transcription (mMESSAGE mMACHINE T7 kit; Ambion) and quantified cRNA concentration spectroscopically (Nano-Drop2000; Thermo Fisher Scientific). We validated the size and integrity of cRNAs using gel electrophoresis (ReliantRNA Gels, 1.25% SeaKem Gold AgaroseSKG; Lonza). To each cRNA sample, we added buffer (2  $\mu$ l 10 $\times$  MOPS buffer; Lonza) and loading dye (8  $\mu$ l, B0363S; NEB) and loaded denatured (70°C, 10 min) samples alongside an RNA ladder (2–4  $\mu$ l, single-strand RNA ladder, N0362S; NEB). The resulting gels were stained with ethidium bromide for 30 min (0.5  $\mu$ g/ml double distilled H<sub>2</sub>O; Thermo Fisher Scientific), washed in double distilled H<sub>2</sub>O (30 min), and visualized with UV light.

*Xenopus* oocytes were isolated from gravid females (NASCO) modified from standard procedures (Liu and Liu, 2006). Briefly, frogs were anesthetized with MS-222 (0.5% buffered with pharmaceutical-grade sodium bicarbonate, pH 7–7.5, 1 h). Follicles were removed, opened with forceps, and transferred to OR-2 solution. For defolliculation, oocytes were incubated (45 min) in OR-2 containing 3 mg/ml collagenase type IV (C-9891; Sigma-Aldrich), washed in fresh OR-2, and incubated in collagenase solution again until follicles were visibly separated from the cells. Defolliculated oocytes were stored in ND96 solution containing (in mM) 96 NaCl, 2.5 KCl, 1 MgCl<sub>2</sub>, 1.8 CaCl<sub>2</sub>, and 5 HEPES, pH 7.6, adjusted with NaOH, containing 10 mg/ml penicillin-streptomycin solution (P0781; Sigma-Aldrich). The OR-2 solution contained (in mM) 82.5 NaCl, 2.5 KCl, 1 MgCl<sub>2</sub>, and 5 HEPES, pH 7.6. We injected cRNA encoding a single DEG/ENaC/ASIC isoform (5 ng) and MEC-2 cRNA (15 ng) in each oocyte. We reduced cRNA amounts to 3 ng (MEC-4d isoforms) and 9 ng (MEC-2) for cells used to collect ibuprofen dose-response curves. We maintained oocytes at 18°C in modified Leibovitz medium (L-15; Sigma-Aldrich) supplemented with gentamicin (144  $\mu$ M; Gibco) and amiloride (300  $\mu$ M) for 2–9 d, as described (Brown et al., 2007). Oocytes expressing UNC-8d were maintained in the same solution with an additional 100  $\mu$ M benzamil. To minimize the impact of variation in the expression of endogenous ion channels and the efficiency of the expression of heterologous channels, we report data from oocytes derived from at least three donor frogs for each channel isoform.

Table 1. Resting membrane potential and properties of membrane current in oocytes expressing DEG/ENaC/ASIC subunits

Channel subunit	$V_{rest}$ (mV)		$V_{rev}$ (mV)		$\Delta V_{rev}$ (mV)	95% CI (mV)		P	Current, $I$ ( $\mu$ A)		95% CI ( $\mu$ A)	P
	Mean $\pm$ SEM (n)	SEM (n)	Mean $\pm$ SEM (n)	SEM (n)		(min, max)	(min, max)		Mean $\pm$ SEM (n)	SEM (n)		
MEC-4d	+13.61 $\pm$ 0.2 (95)		-1.85 $\pm$ 0.114 (93)		47.20	(38.4, 54.7)		2.38e-25	-10.81 $\pm$ 0.085 (95)		(-12.4 to -9.14)	4.53E-39
UNC-8d	+6.93 $\pm$ 0.16 (56)		-3.67 $\pm$ 0.163 (59)		52.80	(44.2, 60.0)		2.85e-20	-1.68 $\pm$ 0.017 (59)		(-1.83 to -1.33)	1.15E-27
DEGT-1d	-19.31 $\pm$ 0.1 (109)		-23.31 $\pm$ 0.140 (111)		25.80	(17.2, 33.3)		9.05e-13	-0.61 $\pm$ 0.004 (113)		(-0.58 to -0.42)	3.08e-34
DEGT-1d alone	-20.87 $\pm$ 3.1 (15)		-23.99 $\pm$ 0.717 (15)		30.8	(21.8, 40.5)		6.56e-05	-0.53 $\pm$ 0.019 (15)		(-0.588 to -0.298)	5.23e-09
DEL-1d	-38.09 $\pm$ 0.9 (18)		-60.68 $\pm$ 1.563 (19)		-11.60	(-26.0, 4.43)		0.166	-0.16 $\pm$ 0.008 (20)		(-0.13 to 0.02)	0.239
MEC-10d	-27.31 $\pm$ 0.92 (19)		-42.12 $\pm$ 1.089 (19)		6.96	(-5.24, 18.7)		0.251	-0.21 $\pm$ 0.009 (19)		(-0.19 to -0.03)	0.004
MEC-2 alone	-48 $\pm$ 7.7 (11)		-67.28 $\pm$ 1.686 (11)		-12.5	(-24.8, 1.2)		0.162	-0.11 $\pm$ 0.004 (11)		(-0.0325 to 0.0257)	0.236
Uninjected	-36.02 $\pm$ 0.12 (143)		-49.08 $\pm$ 0.396 (95)		-	-		-	-0.12 $\pm$ 0.001 (144)		-	-

Mean  $\pm$  SEM for the resting membrane voltage ( $V_{rest}$ ) under current clamp conditions and reversal potential ( $V_{rev}$ ) and current (current,  $I$ ) under voltage clamp conditions at the beginning of each recording session.  $V_{rev}$  was calculated from the ramp protocol in Fig. 1A, and current,  $I$ , was measured at -85 mV. Numbers in parentheses are the total number of oocytes analyzed from at least three donor frogs. Confidence intervals (CIs) are derived from estimation statistics to indicate the effect of channel expression on reversal potential ( $\Delta V_{rev}$ ) and current ( $\Delta I$ ), and exact P values from Mann-Whitney test indicate which conditions generated currents that differed from uninjected control oocytes. Except for MEC-2 and DEGT-1d alone (shown in Fig. S1), these data are drawn from the same data set displayed in graphical form in the lower panels of Fig. 1, I and J.

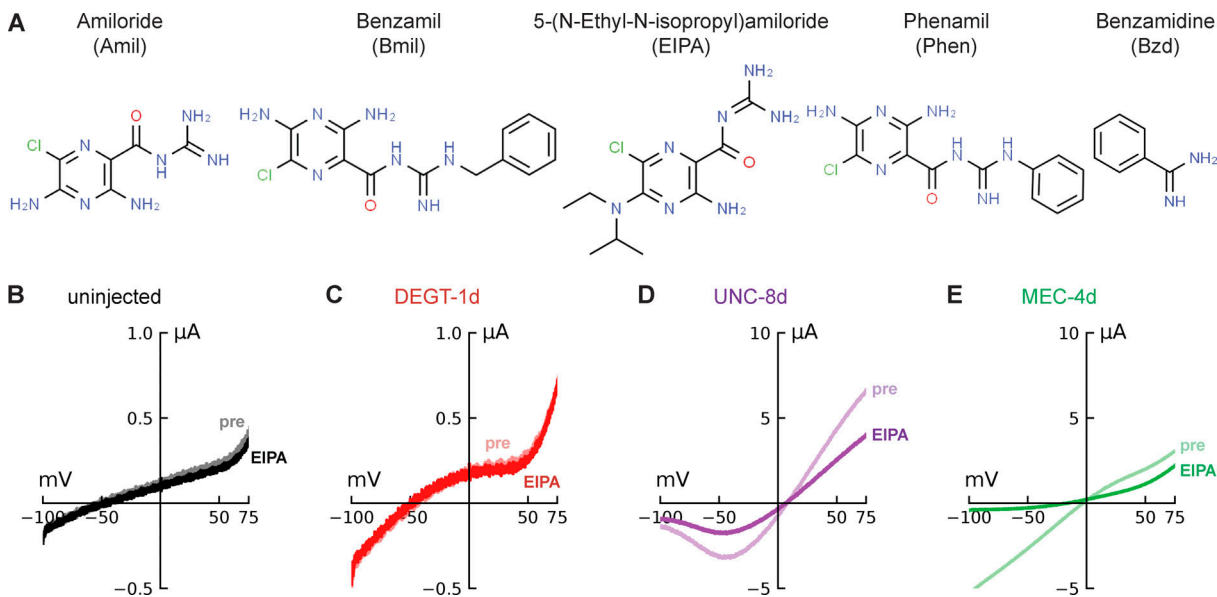


Figure 2. **Structures of amiloride analogues and representative current-voltage curves in the absence (pre) and presence of EIPA.** (A) Structures of amiloride analogues used in this study. (B–E) Current-voltage curves of uninjected oocytes (B) and oocytes coexpressing MEC-2 and DEGT-1d (C), UNC-8d (D), or MEC-4d (E) in the absence (lighter color, pre) and presence (darker color, EIPA) of 30  $\mu\text{M}$  EIPA.

### Whole-cell recordings and external solutions

Membrane current was measured by two-electrode voltage clamp (OC-725C; Warner Instruments, LLC) at room temperature (21–24°C). Electrodes ( $\sim 0.3\text{ M}\Omega$ ) were fabricated from borosilicate glass (G100TF-4; Warner Instruments, LLC) on a horizontal puller (P-97; Sutter Instruments) and filled with 3 M KCl. Analogue signals (current, voltage) were digitized (ITC-16; Instrutech), filtered at 200 Hz (eight-pole Bessel filter), and sampled at 1 kHz. A 60-Hz notch filter (FLA-01; Cygnus Technology, Inc.) was used to reduce line (60 Hz) noise. This equipment was controlled by Patchmaster software (HEKA) on a Windows PC.

Unless otherwise indicated, oocytes were superfused with control saline containing (in mM) 100 Na-gluconate, 2 KCl, 2  $\text{MgCl}_2$ , 1  $\text{CaCl}_2$ , and 10 HEPES, adjusted to pH 7.4 with NaOH. Drugs were diluted from stock solutions and added to control saline. For pH 6.4 and 8.4 solution, we replaced HEPES in the control saline with 10 mM PIPES and 10 mM TAPS, respectively.

We purchased drugs from the indicated suppliers and established stock solutions in DMSO. We used stock solutions of 0.1 M, except for phenamil (0.01 M) and for ibuprofen and aspirin dose–response experiments (0.24 M). Drugs were obtained from these suppliers: amiloride (A7410; Sigma-Aldrich), benzamil (B2417; Sigma-Aldrich), 5-(N-ethyl-N-isopropyl)amiloride (EIPA; A3085; Sigma-Aldrich), phenamil (14308; Cayman Chemical), benzamidine (12072; Fluka), ibuprofen (SLBR3566V; Sigma-Aldrich), R-ibuprofen (16794; Cayman Chemical), S-ibuprofen (375160; Cayman Chemical), aspirin (A2093; Sigma-Aldrich), salicylic acid (S5922; Sigma-Aldrich), diclofenac (D6899; Sigma-Aldrich), and flurbiprofen (F8514; Sigma-Aldrich).

### Measuring current, drug sensitivity, and reversal potential

We used two voltage protocols to measure membrane current and its response to amiloride analogues and NSAIDs (Fig. 1 A): a

voltage ramp (from  $-100$  to  $+100$  mV in 1 s) and voltage steps (from  $-100$  to  $+40$  mV or  $+60$  mV, in 20-mV increments). Both protocols included a conditioning step to  $-85$  mV, which we used to measure current amplitude. In all cases, the holding potential was  $-60$  mV. We applied these protocols repetitively during the application of drugs and solutions with modified ion composition and used voltage ramps to measure reversal potentials.

To determine which channels were indifferent, inhibited, or activated by each of the 10 drugs we tested, we applied each drug a final concentration of 30  $\mu\text{M}$  and measured the difference or drug-sensitive current,  $I_{\text{drug}} = I_{(+\text{drug})} - I_{(-\text{drug})}$ , at  $-85$  mV. Average values were taken from epochs during step and ramp protocols when cells were held at  $-85$  mV (Fig. 1 A, top) and averaged over three voltage presentations in the absence and presence of each drug. Next, we compared  $I_{\text{drug}}$  in experimental and control (uninjected) oocytes, computing the distribution of  $\Delta I_{\text{drug}}$  using estimation statistics (Ho et al., 2019). We used an analogous strategy to assess which channels were indifferent, inhibited, or activated by protons. Specifically, we measured  $I_{\Delta\text{pH}}$  by subtracting the current measured at  $-85$  mV in the presence of pH 6.4 saline from the current measured at pH 8.4, a 100-fold increase in  $\text{H}^+$  concentration. We compared  $I_{\Delta\text{pH}}$  in experimental and control oocytes, computing  $\Delta I_{\Delta\text{pH}}$ . We measured reversal potentials from voltage ramps (Fig. 1 A, top,  $-100$  to  $+100$  mV in 1 s). Drug dose–response curves were measured at voltage steps between  $-100$  and either  $+40$  or  $+60$  mV in 20-mV increment steps. Three replicates of the voltage step protocol were averaged to derive current amplitude in the presence of each drug concentration.

### Data analysis, curve fitting, and figure generation

Mean values and reversal potentials were calculated using MATLAB (R2014b/R2020b; <https://github.com/wormsenseLab/AnalysisFunction.git>).

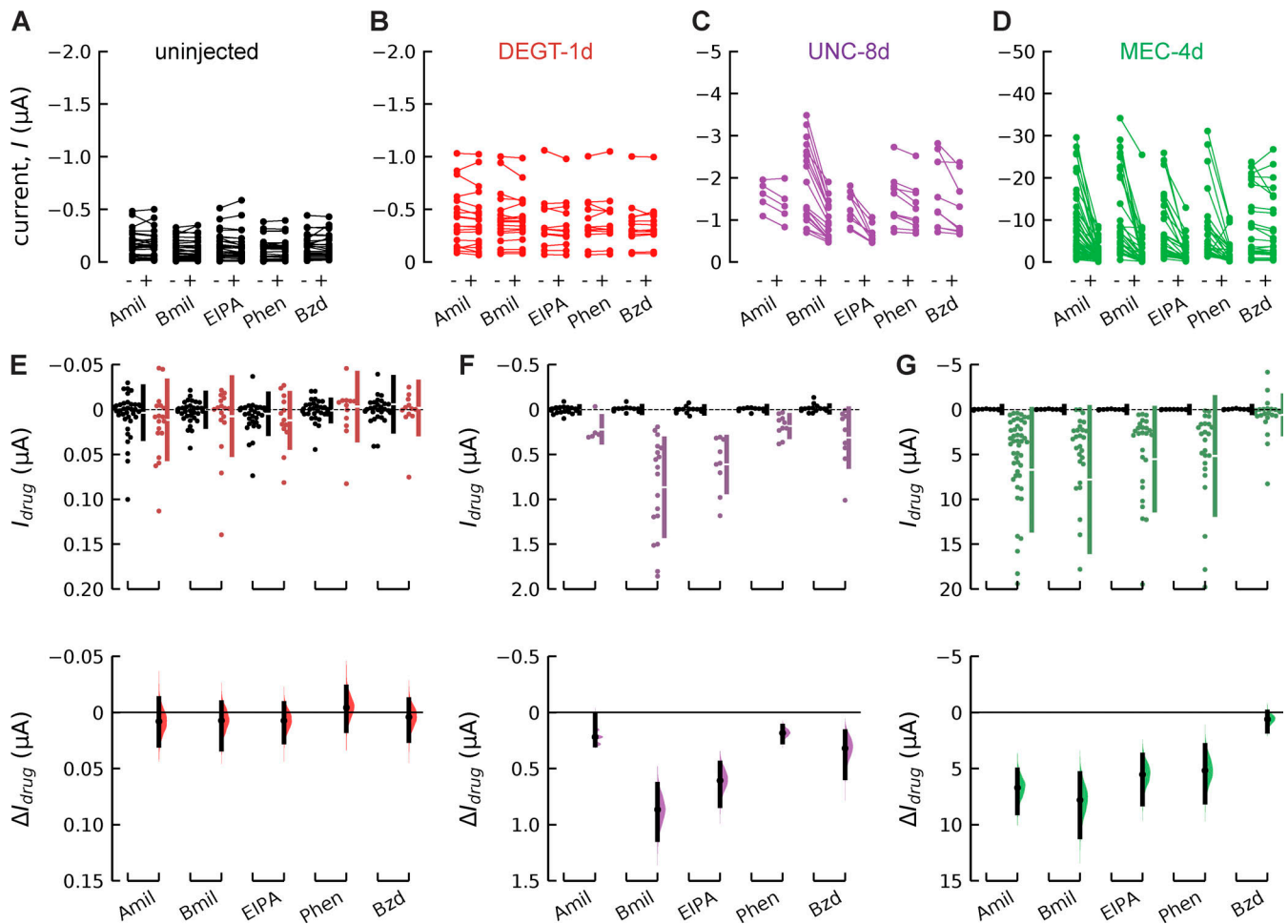


**Figure 3. Unlike MEC-4d and UNC-8d, DEGT-1d currents are insensitive to amiloride analogues. (A–D)** Paired dots show the current at  $-85$  mV in uninjected oocytes (A) and in oocytes coexpressing MEC-2 and DEGT-1d (B), UNC-8d (C), or MEC-4d (D) before and after treatment with  $30 \mu\text{M}$  amiloride (Amil), benzamil (Bmil), EIPA, phenamil (Phen), or benzamidine (Bzd). **(E–G)** Drug-sensitive current ( $I_{\text{drug}}$ ; top) at  $-85$  mV in oocytes expressing DEGT-1d (E), UNC-8d (F), or MEC-4d (G; in color) compared with uninjected oocytes (black). Estimation plots (bottom) showing the effect of each drug ( $\Delta I_{\text{drug}}$ ) on DEGT-1d (E), UNC-8d (F), or MEC-4d (G) relative to the drug effect on uninjected oocytes. Mean values, 95% confidence intervals, and statistical analyses related to E–G are in Table 2, Table 3, and Table 4.

ANOVA (two-way) followed by multiple comparison with the Holm–Sidak method ( $P < 0.05$ ) was performed in Sigma Plot 12.5. Estimation statistics were performed in Python using Data Analysis and Bootstrap-Coupled ESTimation or DABEST (Ho et al., 2019). Using IgorPro 6.37 (Wavemetrics), individual dose response curves were fitted with the Hill equation,  $EC_{50} = I_{\text{max}} * [x^n / (EC_{50}^n + x^n)]$  and  $IC_{50} = I_{\text{max}} * IC_{50}^n / (IC_{50}^n + x^n)$ , where  $EC_{50}$  is the half-maximal concentration for potentiation and  $IC_{50}$  is the half-maximal concentration for inhibition,  $x$  is the drug concentration,  $n$  is the Hill coefficient which was set to 1, and  $I_{\text{max}}$  is the maximum current. We used the mean values for  $EC_{50}$  and  $IC_{50}$  to compute an average fit to the pooled and averaged data. Figures were prepared in python jupyter notebooks (<https://github.com/wormsenseLab/JupyterNotebooksDEGENaCPharm.git>).

### Sequence analysis

The following ion channel sequences (accession nos. in parentheses) were used to generate a phylogenetic tree (see Fig. 7 A) and alignments (Fig. 7 C): ACD-1 (C24G7.2), ACD-2 (C24G7.4),

ACD-3b (C27C12.5b), ACD-4 (F28A12.1), ACD-5 (T28F2.7), ASIC-1 (ZK770.1), ASIC-2 (T28F4.2), DEG-1 (C47C12.6.1), DEGT-1 (F25D1.4), DEL-1 (E02H4.1), DEL-2a (F58G6.6a), DEL-3 (F26A3.6), DEL-4 (T28B8.5), DEL-5 (F59F3.4), DEL-6 (T21C9.3), DEL-7 (C46A5.2), DEL-8 (C11E4.3), DEL-9 (C18B2.6), DEL-10 (T28D9.7), DELM-1 (F23B2.3), DELM-2 (C24G7.1), EGAS-1 (Y69H2.11), EGAS-2 (Y69H2.12), EGAS-3 (Y69H2.2), EGAS-4 (F55G1.13), FLR-1 (F02D10.5), MEC-4 (T01C8.7), MEC-10 (F16F9.5), UNC-8d (R13A1.4d), UNC-105e (C41C4.5e), rASIC-1 (NP\_077068), rASIC-2 (Q62962.1), rASIC-3 (NP\_775158.1), rASIC-4 (Q9JHS6.1),  $\alpha$ ENaC (NP\_113736.1),  $\beta$ ENaC (NP\_036780.1),  $\gamma$ ENaC (NP\_058742.2), and h $\delta$ ENaC (O01123885.2). The alignment for calculating the phylogenetic tree was generated with MUSCL and <http://www.phylogeny.fr> (Dereeper et al., 2010, 2008) and visualized with figtree v1.4.4 (Rambaud, 2018). The alignment was generated with Clustal Omega (Fig. 7 C).

### Online supplemental material

Fig. S1 shows how DEGT-1d is affected by amiloride ibuprofen concentrations  $>30 \mu\text{M}$  as well as how amiloride sensitivity is

Table 2. **Effect of amiloride analogs and NSAIDs on DEGT-1d currents relative to uninjected oocytes: estimation statistics supporting Fig. 3 and Fig. 5**

DEGT-1d	$\Delta I_{drug}$ ( $\mu A$ )	95% CI ( $\mu A$ )	P
<b>Amiloride analogs</b>			
Amiloride	0.0033 (20)	(-0.02 to 0.025)	0.36
Benzamil	0.0073 (18)	(-0.009 to 0.035)	0.61
EIPA	0.0073 (13)	(-0.008 to 0.028)	0.43
Phenamil	-0.0043 (13)	(-0.024 to 0.016)	0.32
Benzamidine	0.0041(13)	(-0.012 to 0.026)	0.77
<b>NSAIDs</b>			
Ibuprofen	0.02 (18)	(0.0068 to 0.036)	0.001
Flurbiprofen	0.15 (5)	(0.084 to 0.22)	0.003
Diclofenac	-0.037 (5)	(-0.075 to -0.015)	0.003
Aspirin	0.037 (5)	(0.0075 to 0.064)	0.08
Salicylic acid	0.073 (4)	(0.042 to 0.094)	0.006

Estimation statistics for Fig. 3 E and Fig. 5 E are described as a change in current ( $\Delta I_{drug}$ ) compared to uninjected oocytes, the 95% CI (in  $\mu A$ ), and a two-sided P value of the Mann-Whitney test. Numbers of experiments are given in parentheses (n).

independent of the presence or absence of MEC-2. Fig. S2 shows the dose-dependence and voltage sensitivity of UNC-8d inhibition by benzamil and MEC-4d inhibition by EIPA.

## Results

We expressed five *C. elegans* DEG/ENaC/ASIC proteins in *Xenopus* oocytes to determine which could form homomeric ion channels. The proteins we studied, DEGT-1d, DEL-1d, UNC-8d, MEC-10d, and MEC-4d, are expressed in three classes of mechanoreceptor neurons: touch receptor neurons, polymodal nociceptors, and stretch-sensitive motor neurons. To increase the likelihood of detecting DEG/ENaC/ASIC-dependent currents, we used mutant or *d* isoforms of each of these proteins linked to neuronal degeneration. We also coexpressed all channel subunits with MEC-2, based on prior studies showing that this yields larger currents than expressing MEC-4d alone (Brown et al., 2007; Goodman et al., 2002; Matthewman et al., 2016; Zhang et al., 2004). Individual proteins were deemed capable of forming homomeric ion channels if total membrane current (measured at -85 mV) and its reversal potential differed from those measured in uninjected control oocytes. We sought additional evidence that each protein formed active channels by measuring the response to a change in pH, sensitivity to amiloride and its analogues, and sensitivity to a panel of NSAIDs.

### DEGT-1d, but not DEL-1d, forms homomeric channels

Previous research showed that the DEG/ENaC/ASIC subunits MEC-4d and UNC-8d, but not MEC-10d, can form homomeric channels when exogenously expressed in *Xenopus* oocytes (Goodman et al., 2002; Wang et al., 2013). Coexpression with MEC-2 increases MEC-4d (Brown et al., 2008; Goodman et al.,

Table 3. **Effect of amiloride analogs and NSAIDs on UNC-8d currents relative to uninjected oocytes: estimation statistics supporting Fig. 3 and Fig. 5**

UNC-8d	$\Delta I_{drug}$ ( $\mu A$ )	95% CI ( $\mu A$ )	P
<b>Amiloride analogs</b>			
Amiloride	0.22 (5)	(0.026 to 0.29)	0.03
Benzamil	0.87 (18)	(0.64 to 1.13)	2.08e-09
EIPA	0.61 (9)	(0.45 to 0.83)	4.92e-06
Phenamil	0.18 (10)	(0.12 to 0.26)	2.86e-06
Benzamidine	0.32 (9)	(0.17 to 0.58)	1.29e-05
<b>NSAIDs</b>			
Ibuprofen	0.026 (15)	(0.000518 to 0.0492)	0.024
Flurbiprofen	0.22 (10)	(0.123 to 0.382)	0.00033
Diclofenac	0.24 (13)	(0.156 to 0.352)	5.25e-06
Aspirin	-0.071 (9)	(-0.162 to 0.00864)	0.39
Salicylic acid	-0.062 (10)	(-0.197 to 0.00931)	0.16

Estimation statistics for Fig. 3 F and Fig. 5 F are described as a change in current ( $\Delta I_{drug}$ ) compared to uninjected oocytes, the 95% CI (in  $\mu A$ ), and a two-sided P value of the Mann-Whitney test. Numbers of experiments are given in parentheses (n).

2002; Matthewman et al., 2016) but not UNC-8d currents (Matthewman et al., 2016). On average, oocytes expressing MEC-4d generated inward currents at -85 mV that were approximately sevenfold larger than those expressing UNC-8d and 17-fold larger than those expressing DEGT-1d. Oocytes expressing MEC-10d and DEL-1d, by contrast, generated currents that were indistinguishable from those recorded in uninjected

Table 4. **Effect of amiloride analogs and NSAIDs on MEC-4d currents relative to uninjected oocytes: estimation statistics supporting Fig. 3 and Fig. 5**

MEC-4d	$\Delta I_{drug}$ ( $\mu A$ )	95% CI ( $\mu A$ )	P
<b>Amiloride analogs</b>			
Amiloride	6.71 (50)	(5.1 to 8.87)	2.07e-15
Benzamil	7.81 (32)	(5.43 to 11.0)	2.03e-12
EIPA	5.53 (27)	(3.77 to 8.11)	2.07e-11
Phenamil	5.18 (26)	(3.1 to 8.08)	2.02e-09
Benzamidine	0.61 (25)	(-0.065 to 1.68)	0.0022
<b>NSAIDs</b>			
Ibuprofen	-4.39 (9)	(-6.43 to -2.69)	0.0015
Flurbiprofen	-3.7 (7)	(-4.66 to -2.92)	0.0008
Diclofenac	-2.78 (24)	(-4.44 to -1.66)	9.91e-08
Aspirin	-4.75 (6)	(-7.73 to -3.45)	0.0014
Salicylic acid	-5.39 (7)	(-7.26 to -3.89)	0.0008

Estimation statistics for Fig. 3 G and Fig. 5 G are described as a change in current ( $\Delta I_{drug}$ ) compared to uninjected oocytes, the 95% CI (in  $\mu A$ ), and a two-sided P value of the Mann-Whitney test. Numbers of experiments are given in parentheses (n).

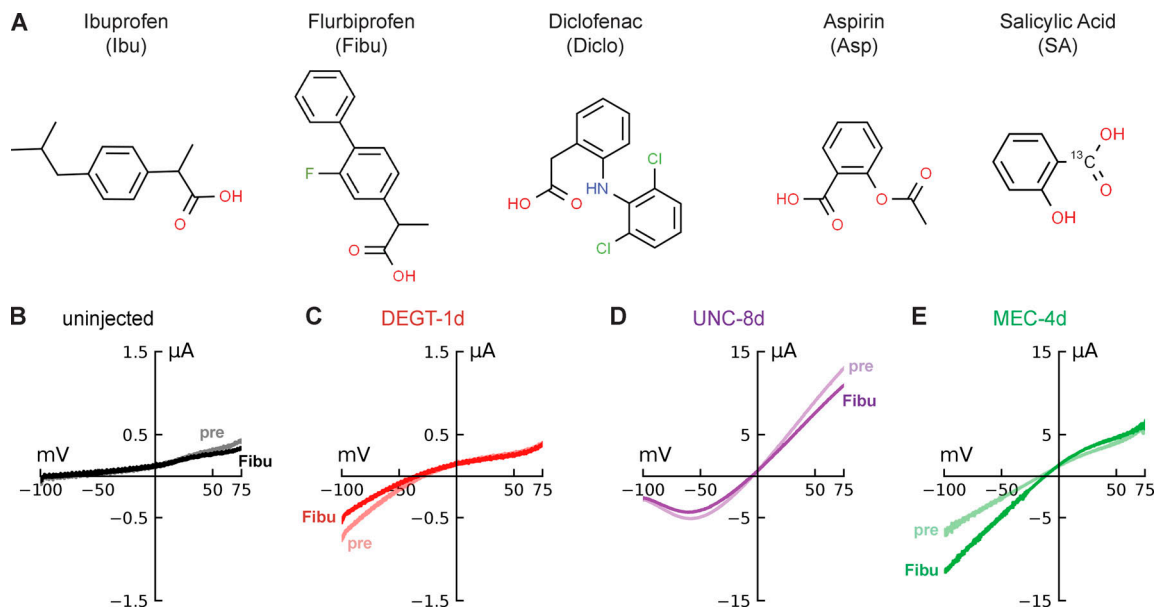


Figure 4. **Structures of NSAIDs and representative current-voltage curves in the absence (pre) and presence of flurbiprofen (Fibu).** (A) Chemical structures of NSAIDs used in this study. (B–E) Current-voltage curves of uninjected oocytes (B) and in oocytes coexpressing MEC-2 and DEGT-1d (C), UNC-8d (D), or MEC-4d (E) in the absence (lighter color) and presence (darker color) of 30  $\mu$ M Fibu.

oocytes (Fig. 1, A–I; and Table 1). Consistent with prior reports that oocytes expressing DEG/ENaC/ASIC channels become sodium-loaded during the incubation period (Brown et al., 2007; Canessa et al., 1994; Goodman et al., 2002), membrane current reversed polarity near 0 mV in oocytes expressing MEC-4d and UNC-8d (Fig. 1, C, D, and I; and Table 1). UNC-8d-expressing oocytes had more positive resting membrane potentials (Table 1) following incubation in a medium containing benzamil (100  $\mu$ M) in addition to amiloride (300  $\mu$ M). With these findings, we replicate prior work showing that MEC-4d and UNC-8d, but not MEC-10d, form homomeric channels in oocytes (Goodman et al., 2002; Wang et al., 2013) and show that DEL-1d is not likely to form ion channels on its own.

Oocytes expressing DEGT-1d generated small currents at  $-85$  mV, and these currents reversed polarity at significantly more positive potentials than those recorded from uninjected cells and those expressing MEC-10d and DEL-1d. The reversal potential of DEGT-1d currents was also significantly more negative than those recorded from cells expressing MEC-4d and UNC-8d (Fig. 1, B–D and I; and Table 1). Together, these findings suggest that DEGT-1d is sufficient to generate an ion channel whose ion permeability appears to differ from channels formed by MEC-4d and UNC-8d. These properties are not conferred by MEC-2, since DEGT-1 currents were indifferent to its presence (Fig. S1 A and Table 1). Similarly, the currents are not conferred by MEC-2, since oocytes expressing MEC-2 alone were indistinguishable from uninjected oocytes (Fig. S1 A and Table 1; Goodman et al., 2002).

To verify that DEGT-1d is able to form homomeric channels, we sought recording conditions in which the current could be potentiated or blocked. As other members of this superfamily form acid-sensitive ion channels, we tested the effect of increasing the extracellular proton concentration on currents carried by DEGT-1d, MEC-4d, and UNC-8d switching from

solutions from pH 8.4 and 6.4. This maneuver decreased current carried by DEGT-1d and, to a lesser degree, MEC-4d, leading to a positive  $I_{\Delta\text{pH}}$  (Fig. 1 J, top). By contrast, acidification appeared to potentiate UNC-8d currents (Fig. 1 J, top). To determine whether these effects differed from that found in control oocytes, we used an estimation approach to compute the distribution of  $\Delta I_{\Delta\text{pH}}$  (effect size and 95% confidence intervals) for each channel type (Fig. 1 J, bottom). Collectively, these findings indicate that DEGT-1d forms a homomeric channel with properties that differ from most other DEG/ENaC/ASIC channels and suggest that alkalization could enhance and acidification could suppress DEGT-1-dependent currents in vivo.

#### Unlike MEC-4d and UNC-8d, DEGT-1d is insensitive to amiloride analogues

The DEG/ENaC/ASIC ion channel family is also known as the amiloride-sensitive ion channel family (Goodman and Schwarz, 2003; Hanukoglu and Hanukoglu, 2016; Kellenberger and Schild, 2002), suggesting that channels formed by these proteins are sensitive to the diuretic amiloride and its derivatives. Indeed, both MEC-4d and UNC-8d are known to be blocked by amiloride (Goodman et al., 2002; Wang et al., 2013). MEC-4d has a micromolar affinity for amiloride, and UNC-8d is approximately eightfold less sensitive to amiloride (Brown et al., 2007; Goodman et al., 2002; Wang et al., 2013). To learn more about amiloride block as a shared but potentially variable property of DEG/ENaC/ASIC channels, we tested DEGT-1d, UNC-8d, and MEC-4d for sensitivity to amiloride and four analogues: benzamil, EIPA, phenamil, and benzamidine (Figs. 2 and 3). These analogues were developed in an effort to generate specificity for ENaCs and  $\text{Na}^+/\text{H}^+$  antiporters, both of which play critical roles in the mammalian kidney and are inhibited by amiloride (Frelin et al., 1987).



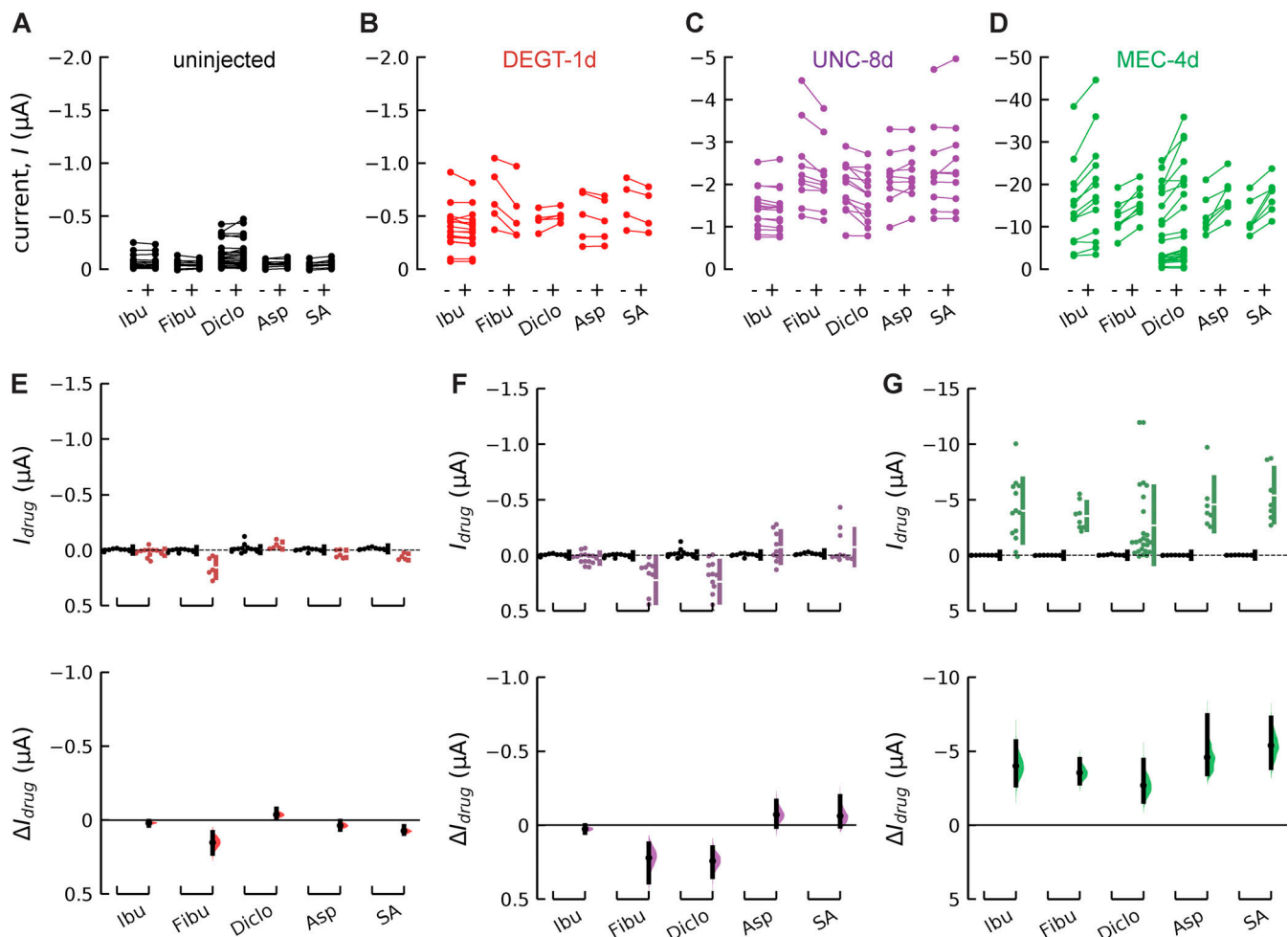


Figure 5. **NSAIDs potentiate MEC-4d current and inhibit or are ineffective on DEGT-1d and UNC-8d.** (A–D) Paired dots show the current at  $-85$  mV in uninjected oocytes (A) and in oocytes coexpressing MEC-2 and DEGT-1d (B), UNC-8d (C), or MEC-4d (D) before and after treatment with  $30$   $\mu\text{M}$  ibuprofen (Ibu), flurbiprofen (Fibu), diclofenac (Diclo), aspirin (Asp), salicylic acid (SA). (E–G) Drug-sensitive current ( $I_{\text{drug}}$ ; top) at  $-85$  mV in oocytes expressing DEGT-1d (E), UNC-8d (F), or MEC-4d (G; in color) compared with uninjected oocytes (black). Estimation plots (bottom) showing the effect of each drug ( $\Delta I_{\text{drug}}$ ) on DEGT-1d (E), UNC-8d (F), or MEC-4d (G) relative to the drug effect on uninjected oocytes. Mean values, 95% confidence intervals, and statistical analyses related to E–G are in Table 2, Table 3, and Table 4.

For simplicity, we exposed oocytes expressing DEGT-1d, UNC-8d, and MEC-4d to a single concentration ( $30$   $\mu\text{M}$ ) of each amiloride analogue. Fig. 2, B–E, shows representative current–voltage curves recorded in the presence and absence of one amiloride analogue, EIPA, in uninjected (control) oocytes and in oocytes expressing each channel. EIPA had no detectable effect on currents in control oocytes or in those expressing DEGT-1d (Fig. 2, A and B). By contrast, EIPA inhibited both UNC-8d and MEC-4d current (Fig. 2, D and E). During each recording, we also measured current amplitude at  $-85$  mV (see voltage protocol, Fig. 1 A, top). Fig. 3, A–D, shows the average current measured in the presence and absence of each analogue for individual control, DEGT-1d, UNC-8d, and MEC-4d oocytes. Next, we determined the drug-sensitive current,  $I_{\text{drug}} = I_{(+\text{drug})} - I_{(-\text{drug})}$ , for each channel isoform and for control oocytes (Fig. 3, E–G, top). Finally, we adopted an estimation statistics approach (Ho et al., 2019) to determine the size of the drug effect,  $\Delta I_{\text{drug}}$ , on DEGT-1d, UNC-8d, and MEC-4d relative to control (Fig. 3, E–G, bottom). See also Table 2, Table 3, and Table 4. In this representation,

negligible effects result in a distribution centered near 0, and inhibitory effects shift the distribution to more positive values.

Unlike MEC-4d, UNC-8d, and most other DEG/ENaC/ASIC channels, DEGT-1d was insensitive to all amiloride analogues we tested at our reference concentration of  $30$   $\mu\text{M}$  (Fig. 3, B and E). To differentiate between a reduced affinity and a lack of sensitivity, we tested concentrations up to  $300$   $\mu\text{M}$  for amiloride. At this concentration, amiloride reduced current in DEGT-1d-expressing oocytes by  $60$  nA, on average, relative to its effect on control oocytes (Fig. S1 A).

UNC-8d is inhibited not only by amiloride and benzamil (Wang et al., 2013; Miller-Fleming et al., 2016) but also by EIPA, phenamil, and benzamidine (Fig. 3, C and F). Amiloride analogues block UNC-8d currents with different degrees of potency. In ascending order of potency, UNC-8d was blocked by amiloride, phenamil, benzamidine, EIPA, and benzamil. The reported  $IC_{50}$  values for UNC-8d channels for amiloride at  $-100$  mV are  $7.8$   $\mu\text{M}$  in divalent-containing and  $106$   $\mu\text{M}$  in divalent-free solution (Wang et al., 2013). The reported  $IC_{50}$  values for UNC-8d

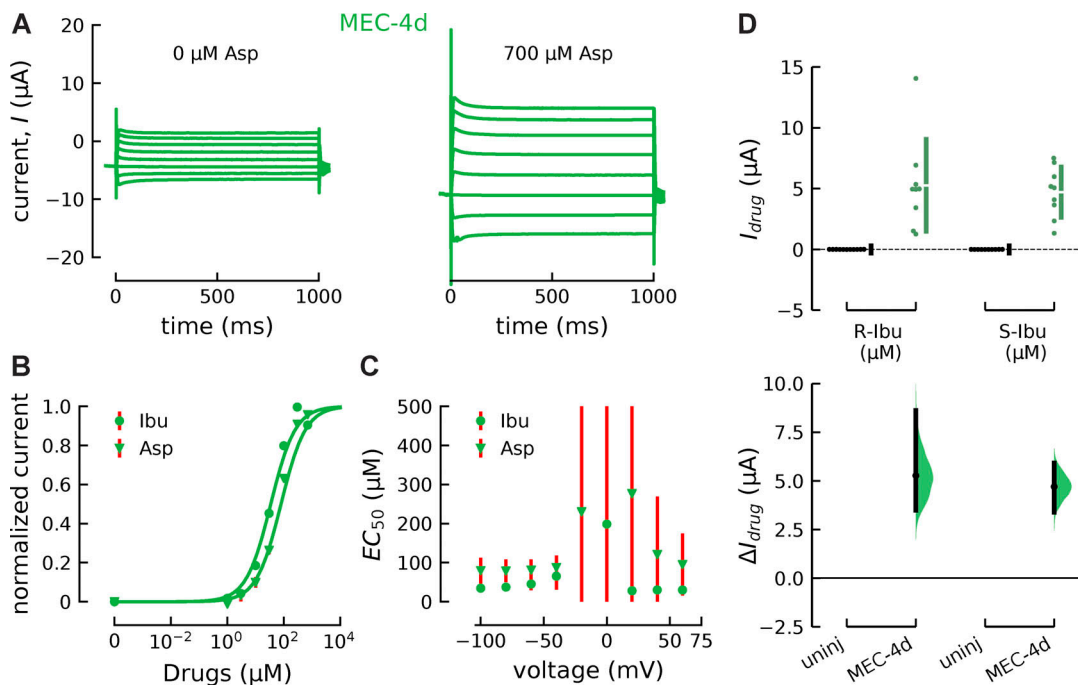


**Figure 6. Sensitivity of MEC-4d channels to NSAIDs ibuprofen and aspirin.** (A) MEC-4d current in the absence (left) and presence of aspirin (Asp, 700  $\mu\text{M}$ ; right). (B) Ibuprofen (Ibu; circles) and aspirin (Asp; triangles) dose–response relationships at  $-100$  mV (normalized to  $I_{\text{max}}$  and baseline current). Points are mean  $\pm$  SEM (Ibu,  $n = 12$ ; Asp,  $n = 9$ ); error bars are smaller than the points in most cases. Smooth lines are fits of the data to the Hill equation (see Materials and methods). (C)  $EC_{50}$  values for different voltages for Ibu (circle) and Asp (triangle). (D) Drug-sensitive MEC-4d current ( $I_{\text{drug}}$ ; top) and estimation plots (bottom) in the presence and absence of ibuprofen isomers (R-Ibu) and (S-Ibu) applied at 30  $\mu\text{M}$  compared with uninjected (uninj) oocytes (black;  $\Delta I_{\text{drug}}$ ). Estimation plots in D (bottom) illustrate the 95% confidence interval (in  $\mu\text{A}$ ), and the two-sided P value of the Mann–Whitney test. The difference for MEC-4d for 30  $\mu\text{M}$  R-Ibu is 5.27  $\mu\text{A}$  (3.49–8.62),  $P = 0.000197$  and for 30  $\mu\text{M}$  S-Ibu is 4.7  $\mu\text{A}$  (3.39–5.91),  $P = 0.00028$ .

channels for benzamil at  $-100$  mV are 47  $\mu\text{M}$  in divalent-containing and 119  $\mu\text{M}$  in divalent-free solution (Miller-Fleming et al., 2016). In this study, we determined an  $IC_{50}$  for benzamil in control saline (divalent-containing solution) of  $14.8 \pm 1.6$   $\mu\text{M}$  ( $n = 4$ ) at  $-60$  mV (15.1  $\mu\text{M}$  at  $-100$  mV; Fig. S2, A–C). In contrast to amiloride inhibition, the apparent affinity to benzamil was indistinguishable at voltages between  $-100$  and  $-20$  mV, indicating that the block by benzamil is not voltage-dependent.

Similar to UNC-8d, MEC-4d is inhibited by amiloride, benzamil, and benzamidine (Brown et al., 2007) and by EIPA and phenamil (Fig. 3, D and G). However, the order of potency differs from UNC-8d. In ascending order, MEC-4d was blocked by benzamidine < amiloride  $\approx$  EIPA  $\approx$  phenamil < benzamil. The similar potency of amiloride and EIPA was unexpected, and we analyzed this drug further by collecting full dose–response curves for EIPA inhibition of MEC-4d (Fig. S2, D–F). The half-blocking dose or  $IC_{50}$  for EIPA was  $3.06 \pm 0.6$   $\mu\text{M}$  ( $n = 11$ ) at  $-60$  mV (Fig. S2, E and F), which is indistinguishable from the  $IC_{50}$  for amiloride ( $2.35 \pm 0.39$   $\mu\text{M}$  [ $n = 7$ ] at  $-60$  mV; Brown et al., 2007). It has been shown that the block through amiloride in ENaC, MEC-4d, and UNC-8d depends on the transmembrane potential difference such that hyperpolarization of the membrane increases channel block (Kellenberger and Schild 2002; Brown et al., 2007; Wang et al., 2013). By comparison, the apparent affinity to EIPA was insensitive to voltage (Fig. S2 F). Collectively, these results show that MEC-4d is blocked by many

amiloride analogues, in this order of potency: benzamidine (196  $\mu\text{M}$ ; Brown et al., 2007) < EIPA (3.06  $\mu\text{M}$ , this study)  $\approx$  amiloride (2.35  $\mu\text{M}$ ; Brown et al., 2007) < benzamil (0.83  $\mu\text{M}$ ; Brown et al., 2007).

If all of these drugs were to function as open channel blockers like amiloride (Brown et al., 2007; Waldmann et al., 1995), then the dramatic difference in their potency among DEGT-1d, UNC-8d, and MEC-4d channels implies that these channels differ in the molecular pathways by which drugs access a common binding site in the pore or that they possess distinct binding sites. We favor the former idea for two reasons. First, the conserved second transmembrane domain of DEG/ENaC/ASIC proteins has long been thought to line the ion conduction pore and to contribute to a conserved amiloride-binding site (Kellenberger et al., 1999; Snyder et al., 1999). Second, access to this site in the pore would be influenced by differences in the open-state conformation of the extracellular domain, and this is the region that is most divergent among the channels we studied.

#### Some NSAIDs block DEGT-1d and UNC-8d, but all potentiate MEC-4d

Because NSAIDs have been reported to block ASIC channels with  $IC_{50}$  values in the high micromolar range (90–350  $\mu\text{M}$ ; Lingueglia and Lazdunski, 2013; Voilley, 2004), we examined sensitivity to five NSAID drugs (Fig. 4 A). This provides an additional window into shared but variable properties of DEG/

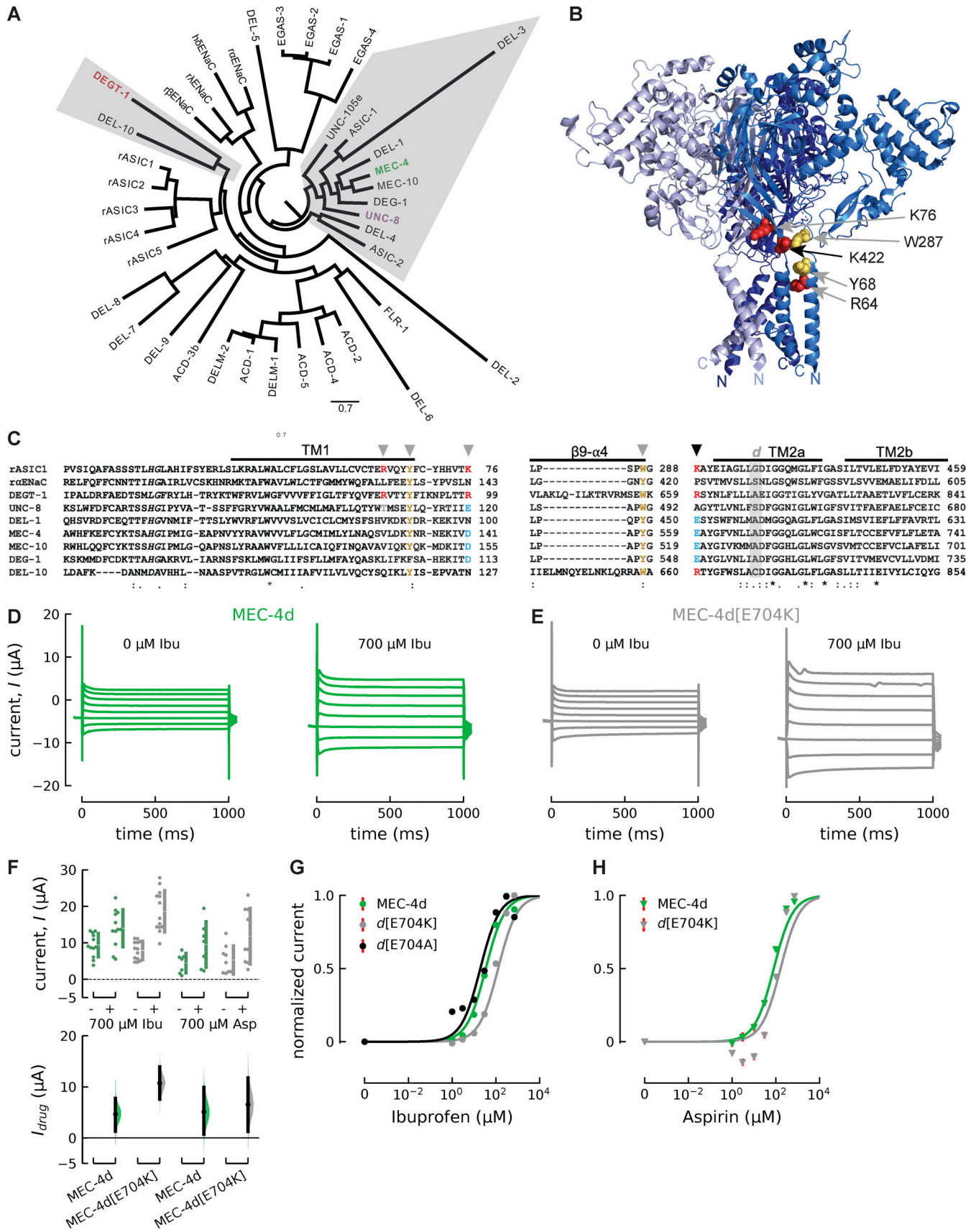


Figure 7. **Amino acid in the wrist close to TM2 in MEC-4d changes sensitivity to ibuprofen and aspirin.** (A) Phylogenetic tree of *C. elegans* DEG/ENaC/ASIC subunits and mammalian ENaC and ASIC subunits. Accession nos. are given in Materials and methods. (B) Ribbon diagram of trimeric cASIC1a (PDB

4NTW) rendered in PyMOL. Residues shown in space-filling mode are linked to ibuprofen binding in rASIC1a (Lynagh et al., 2017). **(C)** Amino acid alignment of rASIC1, rENaC, DEGT-1, UNC-8, MEC-4, DEL-1, MEC-10, DEG-1, and DEL-10 made with Clustal Omega. Left: Amino-terminal domain and transmembrane domain 1 (TM1). Right:  $\beta$ 9- $\alpha$ 4 and transmembrane domain 2 (TM2). Secondary structure motifs numbered as in Jasti et al. (2007). rASIC1a(K422) (black arrowhead) implicated in Ibu sensitivity. The gray *d* indicates the site that mutates to cause degeneration in *C. elegans*. Amino acids implicated in rASIC1 ibuprofen responses are highlighted as follows: red (positively charged), blue (negatively charged), and yellow (hydrophobic). **(D and E)** MEC-4d current traces (D) and MEC-4d(E704K) current (E) in the absence (left) and presence of 700  $\mu$ M (right) ibuprofen (Ibu). **(F)** Current amplitude (current, *I*; top) at  $-85$  mV in the presence and absence of ibuprofen (Ibu) and Aspirin (Asp) for the MEC-4d isoform (green) and the MEC-4d(E704K) isoform (right). Estimation plots (bottom) showing the drug-induced change in current ( $I_{drug}$ ) for MEC-4d (green) or MEC-4d(E704K) (gray) in the presence of 700  $\mu$ M Ibu or Asp compared with the absence of the drugs. Estimation plots show the 95% confidence interval (in  $\mu$ A), and the two-sided P value of the Mann-Whitney test. The effect of 700  $\mu$ M Ibu is 4.63  $\mu$ A (1.29–7.73),  $P = 0.0102$  ( $n = 12$ ) and 10.7  $\mu$ A (7.58–13.9),  $P = 5.09e-05$  ( $n = 13$ ) for MEC-4d and MEC-4d(E704K), respectively. The effect of 700  $\mu$ M Asp is 5.11  $\mu$ A (0.74–9.92),  $P = 0.073$  ( $n = 7$ ) and 6.53  $\mu$ A (1.28–11.8),  $P = 0.0521$  ( $n = 9$ ) for MEC-4d and MEC-4d(E704K), respectively. **(G)** Ibuprofen dose–response relationships for MEC-4d (green), MEC-4d(E704K) (gray), and MEC-4d(E704A) (black) currents at  $-100$  mV (normalized to  $I_{max}$  and baseline current). **(H)** Aspirin dose–response relationships for MEC-4d (green) and MEC-4d-E704K (gray) currents at  $-100$  mV (normalized to  $I_{max}$  and baseline current). Smooth lines in G and H are fits of the data to the Hill equation (see Materials and methods).

ENaC/ASIC channels. Current–voltage curves of uninjected (control), DEGT-1d, UNC-8d, and MEC-4d currents (Fig. 4, B–E) show that ibuprofen has little if any effect on control currents, modestly inhibits DEGT-1d and UNC-8d, and seems to potentiate MEC-4d. None of the NSAIDs tested affected currents in control oocytes at 30  $\mu$ M (Fig. 5 A), providing a simple background for assessing their effect on DEGT-1d, UNC-8d, and MEC-4d.

Similar to our strategy for analyzing the effect of amiloride analogues, we measured current (at  $-85$  mV) in the absence and presence of each NSAID and plotted these paired values for control, DEGT-1d, UNC-8d, and MEC-4d currents (Fig. 5, A–D). Next, we used these data to determine the drug-sensitive current,  $I_{drug}$ , in control and channel-expressing oocytes (Fig. 5, E–G, top) and estimation statistics to determine if the effects exceeded those expected for control oocytes,  $\Delta I_{drug}$  (Fig. 5, E–G, bottom). Collectively, this analysis indicates that 30  $\mu$ M flurbiprofen and salicylic acid partially inhibit DEGT-1 (Fig. 5, B and E) and that 30  $\mu$ M flurbiprofen and diclofenac partially inhibit UNC-8d (Fig. 5, C and F). Higher concentrations of ibuprofen also blocked DEGT-1d currents (Fig. S1 B). Surprisingly, all five NSAIDs potentiated MEC-4d currents (Fig. 5, D and G). See also Table 2, Table 3, and Table 4. These findings demonstrate that NSAIDs can function as antagonists or agonists of DEG/ENaC/ASIC channels, depending on the channel target.

Next, we applied two NSAIDs (ibuprofen and aspirin) to cells expressing MEC-4d channels and analyzed the dose–response relationship as a function of membrane voltage (Fig. 6, A–C). To improve the sensitivity of these measurements, we reduced the baseline currents by injecting 1.6-fold less cRNA encoding MEC-4d for these experiments. Fig. 6 A shows MEC-4d current evoked by a family of voltage steps in the absence (left) and presence (right) of aspirin. The mean  $\pm$  SEM  $EC_{50}$  values for ibuprofen and aspirin at  $-100$  mV are  $34.6 \pm 0.9$   $\mu$ M ( $n = 12$ ) and  $79.9 \pm 3.7$   $\mu$ M ( $n = 9$ ), respectively (Fig. 6 B). Neither drug showed evidence of voltage dependence (Fig. 6 C), suggesting that the binding site for these drugs lies outside the pore region. Ibuprofen is an enantiomer containing two chiral molecules, and the S-isomer is the preferred ligand for its primary targets, the cyclo-oxygenase enzymes COX-1 and COX-2 (Orlando et al., 2015; Selinsky et al., 2001). In contrast, MEC-4d potentiation is equally sensitive to both ibuprofen enantiomers (Fig. 6 D) and is less sensitive to ibuprofen than COX-1 and COX-2 (Blobaum and Marnett, 2007). Collectively, these findings suggest that the

binding sites for NSAIDs differ in DEG/ENaC/ASIC channels and COXs.

MEC-4d is not the only member of the large DEG/ENaC/ASIC ion channel family (Fig. 7 A) affected by NSAIDs. rASIC1a is inhibited by ibuprofen, and this allosteric effect depends on three positively charged and two hydrophobic residues near the first and second transmembrane domains (Fig. 7, B and C; Lynagh et al., 2017). The putative binding site for ibuprofen is proposed to include these five residues. To learn more, we aligned and compared the sequences of seven *C. elegans* DEG/ENaC/ASIC channels with rASIC1a (Fig. 7 C). We found that MEC-4 differs from rASIC1a at the three of the five residues linked to inhibition by ibuprofen (Fig. 7 C, arrowheads). Here, we focused on K422 in rASIC1a and E704, the homologous position in MEC-4 (Fig. 7 C, black arrowhead). Comparing the effect of ibuprofen on MEC-4d and MEC-4d(E704K), we found that ibuprofen potentiated both isoforms (Fig. 7, D and E). We quantified this effect by collecting dose–response curves for ibuprofen and aspirin (Fig. 7 G and H). Sensitivity to ibuprofen was modestly increased in MEC-4d(E704K), but unaffected in MEC-4d(E704A): the mean  $\pm$  SEM  $EC_{50}$  values to ibuprofen for MEC-4d(E704K) and MEC-4d(E704A) at  $-100$  mV are  $135 \pm 40$   $\mu$ M ( $n = 13$ ) and  $19.5 \pm 8.84$   $\mu$ M ( $n = 14$ ), respectively (Fig. 7 G). A similar shift was observed for potentiation for MEC-4d(E704K) by aspirin with a mean  $\pm$  SEM  $EC_{50}$  value of  $179 \pm 56$   $\mu$ M ( $n = 9$ ; Fig. 7 H). This finding differs from allosteric inhibition of rASIC1a, which is significantly impaired by introducing alanine into this position (Lynagh et al., 2017). In an effort to discover the domains responsible for these differences between rASIC1a and MEC-4d, we designed constructs encoding chimeras of these two channels. These chimeras did not generate any detectable current, however, even when coexpressed with MEC-2. The ability of ibuprofen to potentiate MEC-4d and to inhibit rASIC1a could reflect the existence of distinct binding sites in the two channel isoforms or a common, conserved binding site and distinct energetic coupling between ibuprofen binding and channel gating. Based on the similar effects of mutagenesis on apparent ibuprofen affinity, we favor a simple model in which NSAIDs share a similar binding site in MEC-4d and rASIC1a. Future studies to directly determine the ibuprofen-binding sites will be required to differentiate between these classes of models, however.

## Discussion

### Sensitivity to amiloride and its analogues

Developed in 1967 to treat hypertension, amiloride is listed an essential medicine by the [World Health Organization \(2019\)](#). Many amiloride derivatives have been developed, and we leveraged this collection to evaluate the sensitivity of DEGT-1d, UNC-8d, and MEC-4d to a panel of five amiloride analogues ([Figs. 2 and 3](#)). Whereas both MEC-4d and UNC-8d were inhibited by at least one amiloride analogue, DEGT-1d was not obviously affected by any of the five amiloride analogues we tested. UNC-8d currents differed from MEC-4d in their sensitivity to amiloride analogues. In particular, UNC-8d currents are more sensitive to inhibition by benzamil and EIPA than to either amiloride or phenamil. Four of the five compounds inhibited currents carried by MEC-4d (benzamidine had little or no effect on MEC-4d at 30  $\mu$ M, but does block MEC-4d currents at higher doses [[Brown et al., 2007](#)]). Benzamil was the most potent inhibitor of MEC-4d currents, followed by amiloride and EIPA ([Fig. 3 G](#); [Brown et al., 2007](#)). Single-channel recordings demonstrate that amiloride functions as an open channel blocker of MEC-4 channels ([Brown et al., 2007](#)), indicating that amiloride binds within the ion conduction pore. This idea is reinforced by three-dimensional cocrystal structures of cASIC1a and amiloride revealing an amiloride molecule lodged near the external vestibule of the central pore ([Baconguis et al., 2014](#)). Together, our findings suggest that DEGT-1d, UNC-8d, and MEC-4d proteins form homomeric channels that differ in the structure of the amiloride-binding site or in the accessibility of compounds to this site.

### Sensitivity to NSAIDs and their analogues

The mechanism by which NSAIDs generate analgesia is by inhibiting COX-1 and COX-2 enzymes ([Day and Graham, 2013](#); [Weissmann, 1991](#)). These compounds also inhibit DEG/ENaC/ASIC channels ([Lingueglia and Lazdunski, 2013](#); [Lynagh et al., 2017](#); [Voilley, 2004](#); [Voilley et al., 2001](#)) and P2X channels ([Lynagh et al., 2017](#)). We built on these observations and tested *C. elegans* DEG/ENaC/ASICs for sensitivity to a panel of five NSAIDs ([Figs. 4 and 5](#)). Two of the five NSAIDs modestly inhibited DEGT-1d ([Fig. 5 E](#) and [Fig. S1](#)) and UNC-8d ([Fig. 5 F](#)). In contrast with our finding and the well-characterized inhibition of ASIC1a by NSAIDs, all five compounds strongly activated MEC-4d currents ([Fig. 5 G](#)).

Ibuprofen potentiates MEC-4d currents in a dose-dependent manner ([Fig. 6 B](#)) and functions as a negative allosteric modulator of proton-gated ASIC1a currents ([Lynagh et al., 2017](#)). Based on our finding that mutating E704 in MEC-4d decreases the apparent affinity for ibuprofen ([Fig. 7 G](#)), we propose that MEC-4d shares an ibuprofen-binding site with ASIC1a. This raises the question of how ibuprofen binding might enhance MEC-4d current and suppress ASIC1a current. In ASIC1a, ibuprofen and protons elicit opposing conformational changes at the top of the pore-lining second transmembrane domain ([Lynagh et al., 2017](#)), supporting the idea that ibuprofen is a negative allosteric modulator of proton-dependent ASIC1a gating. If a similar conformational change were associated with NSAID binding to MEC-4d, then it would be uncoupled to proton binding (MEC-4d is not activated by protons), and we would

infer that the motion is associated with an increase in channel gating. Future work will be needed to resolve the exact nature of the allosteric interactions between ibuprofen binding and channel gating, however. The differential response of MEC-4d and ASIC1a presents an avenue for further study.

### Concluding remarks

The DEG/ENaC/ASIC channels differ from most if not all other classes of ion channels: they are only present in metazoan genomes ([Katta et al., 2015](#); [Liebeskind et al., 2015](#)). Phylogenetic studies indicate that this gene superfamily has undergone expansions within certain animal lineages, including nematodes and insects ([Liebeskind et al., 2015](#)). By analyzing a subset of *C. elegans* DEG/ENaC/ASIC proteins, we extend understanding of the functional diversification of this ion channel superfamily. In particular, we show that DEGT-1d appears to lack sensitivity to amiloride and four of its derivatives. To our knowledge, this is the first member of this family found to have these properties. This finding suggests that using only amiloride might well obscure the contribution of DEG/ENaC/ASIC channels to cell and tissue function. From the subset of DEG/ENaC/ASIC channels studied, DEGT-1 is phylogenetically distant from the others ([Fig. 7 A](#)). We also identified NSAIDs as potential inhibitors of DEGT-1d and UNC-8d currents and positive activators of MEC-4d currents. Thus, ibuprofen might serve as a tool to screen for the activity of other DEG/ENaC/ASICs in heterologous cells or in their native tissue. Collectively, we demonstrate that each of the proteins able to form homomeric channels in *Xenopus* oocytes exhibits a unique pharmacological footprint within two drug families. This property opens the door to using sensitivity to amiloride and ibuprofen to determine the composition of heterotrimeric DEG/ENaC/ASIC channels either in heterologous cells or in their native tissues.

### Acknowledgments

Jeanne M. Nerbonne served as editor.

We thank Z. Liao for excellent technical support, including *Xenopus* oocyte isolation and molecular biology; and L. Bianchi for the gift of the UNC-8-encoding plasmid.

This work was funded by a fellowship to S. Fechner (Deutsche Forschungsgemeinschaft), the Amgen Scholars Program to I. D'Alessandro (Stanford Summer Research Program), grants from the National Institutes of Health to M.B. Goodman (R01NS07715 and R35NS105092), and support from Howard Hughes Medical Institute to L. Tao.

The authors declare no competing financial interests.

Author contributions: S. Fechner and M.B. Goodman conceived the project. S. Fechner, I. D'Alessandro, and M.B. Goodman designed research. S. Fechner, I. D'Alessandro, L. Wang, and C. Tower performed research. L. Tao contributed new reagents. S. Fechner, I. D'Alessandro, and C. Tower analyzed data. S. Fechner created figures. S. Fechner and M.B. Goodman wrote the paper. I. D'Alessandro, L. Wang, C. Tower, and L. Tao edited the paper.

Submitted: 8 May 2020

Accepted: 12 January 2021

## References

- Adams, C.M., P.M. Snyder, and M.J. Welsh. 1999. Paradoxical stimulation of a DEG/ENaC channel by amiloride. *J. Biol. Chem.* 274:15500–15504. <https://doi.org/10.1074/jbc.274.22.15500>
- Baconguis, I., C.J. Bohlen, A. Goehring, D. Julius, and E. Gouaux. 2014. X-ray structure of acid-sensing ion channel 1-snake toxin complex reveals open state of a Na<sup>+</sup>-selective channel. *Cell.* 156:717–729. <https://doi.org/10.1016/j.cell.2014.01.011>
- Blobaum, A.L., and L.J. Marnett. 2007. Structural and functional basis of cyclooxygenase inhibition. *J. Med. Chem.* 50:1425–1441. <https://doi.org/10.1021/jm0613166>
- Boscardin, E., O. Alijevic, E. Hummler, S. Frateschi, and S. Kellenberger. 2016. The function and regulation of acid-sensing ion channels (ASICs) and the epithelial Na<sup>+</sup> channel (ENaC): IUPHAR Review 19. *Br. J. Pharmacol.* 173:2671–2701. <https://doi.org/10.1111/bph.13533>
- Brown, A.L., S.M. Fernandez-Illescas, Z. Liao, and M.B. Goodman. 2007. Gain-of-function mutations in the MEC-4 DEG/ENaC sensory mechanotransduction channel alter gating and drug blockade. *J. Gen. Physiol.* 129:161–173. <https://doi.org/10.1085/jgp.200609672>
- Brown, A.L., Z. Liao, and M.B. Goodman. 2008. MEC-2 and MEC-6 in the *Caenorhabditis elegans* sensory mechanotransduction complex: auxiliary subunits that enable channel activity. *J. Gen. Physiol.* 131:605–616. <https://doi.org/10.1085/jgp.200709910>
- Canessa, C.M., L. Schild, G. Buell, B. Thorens, I. Gautschi, J.-D. Horisberger, and B.C. Rossier. 1994. Amiloride-sensitive epithelial Na<sup>+</sup> channel is made of three homologous subunits. *Nature.* 367:463–467. <https://doi.org/10.1038/367463a0>
- Canessa, C.M., J.D. Horisberger, L. Schild, and B.C. Rossier. 1995. Expression cloning of the epithelial sodium channel. In *Kidney International. Department of Cellular and Molecular Physiology, Yale School of Medicine, New Haven, CT.* 950–955. <https://doi.org/10.1038/ki.1995.376>
- Chalfie, M., and E. Wolinsky. 1990. The identification and suppression of inherited neurodegeneration in *Caenorhabditis elegans*. *Nature.* 345:410–416. <https://doi.org/10.1038/345410a0>
- Chalfie, M., D.S. Chelur, G.G. Ernstrom, R. O'Hagan, C.A. Yao, and M.B. Goodman. 2003. METHODS AND COMPOSITIONS FOR PROPAGATING VECTORS CONTAINING TOXIC cDNAs AND ION CHANNEL ASSAY SYSTEMS. World Intellectual Property Organization patent WO/2003/060093A2, filed January 8, 2003, and issued January 1, 2004.
- Chatzigeorgiou, M., S. Yoo, J.D. Watson, W.H. Lee, W.C. Spencer, K.S. Kindt, S.W. Hwang, D.M. Miller, III, M. Treinin, M. Driscoll, et al. 2010. Specific roles for DEG/ENaC and TRP channels in touch and thermosensation in *C. elegans* nociceptors. *Nat. Neurosci.* 13:861–868. <https://doi.org/10.1038/nn.2581>
- Dawson, R.J.P., J. Benz, P. Stohler, T. Tetaz, C. Joseph, S. Huber, G. Schmid, D. Hügin, P. Pflimlin, G. Trube, et al. 2012. Structure of the acid-sensing ion channel 1 in complex with the gating modifier Psalmotoxin 1. *Nat. Commun.* 3:936. <https://doi.org/10.1038/ncomms1917>
- Day, R.O., and G.G. Graham. 2013. Non-steroidal anti-inflammatory drugs (NSAIDs). *BMJ.* 346:f3195. <https://doi.org/10.1136/bmj.f3195>
- Dereeper, A., V. Guignon, G. Blanc, S. Audic, S. Buffet, F. Chevenet, J.F. Dufayard, S. Guindon, V. Lefort, M. Lescot, et al. 2008. Phylogeny.fr: robust phylogenetic analysis for the non-specialist. *Nucleic Acids Res.* 36(Web Server, Web Server issue):W465–9. <https://doi.org/10.1093/nar/gkn180>
- Dereeper, A., S. Audic, J.M. Claverie, and G. Blanc. 2010. BLAST-EXPLORER helps you building datasets for phylogenetic analysis. *BMC Evol. Biol.* 10:8–13. <https://doi.org/10.1186/1471-2148-10-8>
- Driscoll, M., and M. Chalfie. 1991. The *mec-4* gene is a member of a family of *Caenorhabditis elegans* genes that can mutate to induce neuronal degeneration. *Nature.* 349:588–593. <https://doi.org/10.1038/349588a0>
- Eastwood, A.L., and M.B. Goodman. 2012. Insight into DEG/ENaC channel gating from genetics and structure. *Physiology (Bethesda).* 27:282–290. <https://doi.org/10.1152/physiol.00006.2012>
- Elkhatib, W., C.L. Smith, and A. Senatore. 2019. A Na<sup>+</sup> leak channel cloned from *Trichoplax adhaerens* extends extracellular pH and Ca<sup>2+</sup> sensing for the DEG/ENaC family close to the base of Metazoa. *J. Biol. Chem.* 294:16320–16336. <https://doi.org/10.1074/jbc.RA119.010542>
- Frelin, C., P. Vigne, P. Barbry, and M. Lazdunski. 1987. Molecular properties of amiloride action and of its Na<sup>+</sup> transporting targets. *Kidney Int.* 32:785–793. <https://doi.org/10.1038/ki.1987.277>
- García-Añoveros, J., B. Derfler, J. Neville-Golden, B.T. Hyman, and D.P. Corey. 1997. BNaC1 and BNaC2 constitute a new family of human neuronal sodium channels related to degenerins and epithelial sodium channels. *Proc. Natl. Acad. Sci. USA.* 94:1459–1464. <https://doi.org/10.1073/pnas.94.4.1459>
- Garty, H., and D.J. Benos. 1988. Characteristics and regulatory mechanisms of the amiloride-blockable Na<sup>+</sup> channel. *Physiol. Rev.* 68:309–373. <https://doi.org/10.1152/physrev.1988.68.2.309>
- Gonzales, E.B., T. Kawate, and E. Gouaux. 2009. Pore architecture and ion sites in acid-sensing ion channels and P2X receptors. *Nature.* 460:599–604. <https://doi.org/10.1038/nature08218>
- Goodman, M.B., and E.M. Schwarz. 2003. Transducing touch in *Caenorhabditis elegans*. *Annu. Rev. Physiol.* 65:429–452. <https://doi.org/10.1146/annurev.physiol.65.092101.142659>
- Goodman, M.B., G.G. Ernstrom, D.S. Chelur, R. O'Hagan, C.A. Yao, and M. Chalfie. 2002. MEC-2 regulates *C. elegans* DEG/ENaC channels needed for mechanosensation. *Nature.* 415:1039–1042. <https://doi.org/10.1038/4151039a>
- Hanukoglu, I., and A. Hanukoglu. 2016. Epithelial sodium channel (ENaC) family: Phylogeny, structure-function, tissue distribution, and associated inherited diseases. *Gene.* 579:95–132. <https://doi.org/10.1016/j.gene.2015.12.061>
- Ho, J., T. Tumkaya, S. Aryal, H. Choi, and A. Claridge-Chang. 2019. Moving beyond P values: data analysis with estimation graphics. *Nat. Methods.* 16:565–566. <https://doi.org/10.1038/s41592-019-0470-3>
- Hobert, O. 2013. The neuronal genome of *Caenorhabditis elegans*. *WormBook.* 1–106. <https://doi.org/10.1895/wormbook.1.161.1>
- Huang, M., and M. Chalfie. 1994. Gene interactions affecting mechanosensory transduction in *Caenorhabditis elegans*. *Nature.* 367:467–470. <https://doi.org/10.1038/367467a0>
- Jasti, J., H. Furukawa, E.B. Gonzales, and E. Gouaux. 2007. Structure of acid-sensing ion channel 1 at 1.9 Å resolution and low pH. *Nature.* 449:316–323. <https://doi.org/10.1038/nature06163>
- Katta, S., M. Krieg, and M.B. Goodman. 2015. Feeling force: physical and physiological principles enabling sensory mechanotransduction. *Annu Rev Cell Dev Biol.* 31:347–371. <https://doi.org/10.1146/annurev-cellbio-100913-013426>
- Kellenberger, S., and L. Schild. 2002. Epithelial sodium channel/degenerin family of ion channels: a variety of functions for a shared structure. *Physiol. Rev.* 82:735–767. <https://doi.org/10.1152/physrev.00007.2002>
- Kellenberger, S., and L. Schild. 2015. International Union of Basic and Clinical Pharmacology. XCI. structure, function, and pharmacology of acid-sensing ion channels and the epithelial Na<sup>+</sup> channel. *Pharmacol. Rev.* 67:1–35. <https://doi.org/10.1124/pr.114.009225>
- Kellenberger, S., I. Gautschi, and L. Schild. 1999. A single point mutation in the pore region of the epithelial Na<sup>+</sup> channel changes ion selectivity by modifying molecular sieving. *Proc. Natl. Acad. Sci. USA.* 96:4170–4175. <https://doi.org/10.1073/pnas.96.7.4170>
- Liesbeskind, B.J., D.M. Hillis, and H.H. Zakon. 2015. Convergence of ion channel genome content in early animal evolution. *Proc. Natl. Acad. Sci. USA.* 112:E846–E851. <https://doi.org/10.1073/pnas.1501195112>
- Liman, E.R., J. Tytgat, and P. Hess. 1992. Subunit stoichiometry of a mammalian K<sup>+</sup> channel determined by construction of multimeric cDNAs. *Neuron.* 9:861–871. [https://doi.org/10.1016/0896-6273\(92\)90239-A](https://doi.org/10.1016/0896-6273(92)90239-A)
- Linguaglia, E., and M. Lazdunski. 2013. Pharmacology of ASIC channels. *Wiley Interdiscip. Rev. Membr. Transp. Signal.* 2:155–171. <https://doi.org/10.1002/wmts.88>
- Liu, X.S., and X.J. Liu. 2006. Xenopus protocols cell biology and signal transduction. *Methods Mol. Biol.* 322. <https://doi.org/10.1007/978-1-59745-000-3>
- Liu, P., B. Chen, and Z.-W. Wang. 2020. GABAergic motor neurons bias locomotor decision-making in *C. elegans*. *Nat. Commun.* 11:5076. <https://doi.org/10.1038/s41467-020-18893-9>
- Lynagh, T., J.L. Romero-Rojo, C. Lund, and S.A. Pless. 2017. Molecular basis for allosteric inhibition of acid-sensing ion channel 1a by ibuprofen. *J. Med. Chem.* 60:8192–8200. <https://doi.org/10.1021/acs.jmedchem.7b01072>
- Matthewman, C., T.W. Miller-Fleming, D.M. Miller, and L. Bianchi. 2016. Ca<sup>2+</sup> permeability and Na<sup>+</sup> conductance in cellular toxicity caused by hyperactive DEG/ENaC channels. *Am. J. Physiol. Cell Physiol.* 311:C920–C930. <https://doi.org/10.1152/ajpcell.00247.2016>
- Matthewman, C., C.K. Johnson, D.M. Miller III, and L. Bianchi. 2018. Functional features of the “finger” domain of the DEG/ENaC channels MEC-4 and UNC-8. *Am. J. Physiol. Cell Physiol.* 315:C155–C163. <https://doi.org/10.1152/ajpcell.00297.2017>
- Miller-Fleming, T.W., S.C. Petersen, L. Manning, C. Matthewman, M. Gornet, A. Beers, S. Hori, S. Mitani, L. Bianchi, J. Richmond, and D.M. Miller. 2016. The DEG/ENaC cation channel protein UNC-8 drives activity-dependent synapse removal in remodeling GABAergic neurons. *eLife.* 5:e14599. <https://doi.org/10.7554/eLife.14599>

- Noreng, S., A. Bharadwaj, R. Posert, C. Yoshioka, and I. Bacongus. 2018. Structure of the human epithelial sodium channel by cryo-electron microscopy. *eLife*. 7:e39340. <https://doi.org/10.7554/eLife.39340>
- O'Hagan, R., M. Chalfie, and M.B. Goodman. 2005. The MEC-4 DEG/ENaC channel of *Caenorhabditis elegans* touch receptor neurons transduces mechanical signals. *Nat. Neurosci.* 8:43–50. <https://doi.org/10.1038/nn1362>
- Orlando, B.J., M.J. Lucido, and M.G. Malkowski. 2015. The structure of ibuprofen bound to cyclooxygenase-2. *J. Struct. Biol.* 189:62–66. <https://doi.org/10.1016/j.jsb.2014.11.005>
- Palmer, L.G. 1992. Epithelial Na channels: function and diversity. *Annu. Rev. Physiol.* 54:51–66. <https://doi.org/10.1146/annurev.ph.54.030192.000411>
- Rambaud, A. 2018. FigTree 1.4.4 Software. <http://tree.bio.ed.ac.uk/software/figtree/>
- Schild, L., E. Schneeberger, I. Gautschi, and D. Firsov. 1997. Identification of amino acid residues in the alpha, beta, and gamma subunits of the epithelial sodium channel (ENaC) involved in amiloride block and ion permeation. *J. Gen. Physiol.* 109:15–26. <https://doi.org/10.1085/jgp.109.1.15>
- Selinsky, B.S., K. Gupta, C.T. Sharkey, and P.J. Loll. 2001. Structural analysis of NSAID binding by prostaglandin H2 synthase: time-dependent and time-independent inhibitors elicit identical enzyme conformations. *Biochemistry*. 40:5172–5180. <https://doi.org/10.1021/bi010045s>
- Snyder, P.M., D.R. Olson, and D.B. Bucher. 1999. A pore segment in DEG/ENaC Na(+) channels. *J. Biol. Chem.* 274:28484–28490. <https://doi.org/10.1074/jbc.274.40.28484>
- Sun, D., Y. Yu, X. Xue, M. Pan, M. Wen, S. Li, Q. Qu, X. Li, L. Zhang, X. Li, et al. 2018. Cryo-EM structure of the ASIC1a-mambalgin-1 complex reveals that the peptide toxin mambalgin-1 inhibits acid-sensing ion channels through an unusual allosteric effect. *Cell Discov.* 4:27. <https://doi.org/10.1038/s41421-018-0026-1>
- Tao, L., D. Porto, Z. Li, S. Fechner, S.A. Lee, M.B. Goodman, X.Z.S. Xu, H. Lu, and K. Shen. 2019. Parallel processing of two mechanosensory modalities by a single neuron in *C. elegans*. *Dev. Cell.* 51:617–631.e3. <https://doi.org/10.1016/j.devcel.2019.10.008>
- Tavernarakis, N., W. Shreffler, S. Wang, and M. Driscoll. 1997. *unc-8*, a DEG/ENaC family member, encodes a subunit of a candidate mechanically gated channel that modulates *C. elegans* locomotion. *Neuron*. 18:107–119. [https://doi.org/10.1016/S0896-6273\(01\)80050-7](https://doi.org/10.1016/S0896-6273(01)80050-7)
- Voilley, N. 2004. Acid-sensing ion channels (ASICs): new targets for the analgesic effects of non-steroid anti-inflammatory drugs (NSAIDs). *Curr. Drug Targets Inflamm. Allergy.* 3:71–79. <https://doi.org/10.2174/1568010043483980>
- Voilley, N., J. de Weille, J. Mamet, and M. Lazdunski. 2001. Nonsteroid anti-inflammatory drugs inhibit both the activity and the inflammation-induced expression of acid-sensing ion channels in nociceptors. *J. Neurosci.* 21:8026–8033. <https://doi.org/10.1523/JNEUROSCI.21-20-08026.2001>
- Vullo, S., and S. Kellenberger. 2019. A molecular view of the function and pharmacology of acid-sensing ion channels. *Pharmacol. Res.* 0–1. <https://doi.org/10.1016/j.phrs.2019.02.005>
- Waldmann, R., G. Champigny, F. Bassilana, N. Voilley, and M. Lazdunski. 1995. Molecular cloning and functional expression of a novel amiloride-sensitive Na+ channel. *J. Biol. Chem.* 270:27411–27414. <https://doi.org/10.1074/jbc.270.46.27411>
- Waldmann, R., G. Champigny, F. Bassilana, C. Heurteaux, and M. Lazdunski. 1997. A proton-gated cation channel involved in acid-sensing. *Nature*. 386:173–177. <https://doi.org/10.1038/386173a0>
- Wang, Y., C. Matthewman, L. Han, T. Miller, D.M. Miller, III, and L. Bianchi. 2013. Neurotoxic *unc-8* mutants encode constitutively active DEG/ENaC channels that are blocked by divalent cations. *J. Gen. Physiol.* 142:157–169. <https://doi.org/10.1085/jgp.201310974>
- Weissmann, G. 1991. The actions of NSAIDs. *Hosp. Pract. (Off. Ed.)*. 26:60–76. <https://doi.org/10.1080/21548331.1991.11705279>
- World Health Organization. 2019. Additions and deletions of medicines on the WHO model lists of essential medicines: 1977–2017. World Health Organization
- Yoder, N., C. Yoshioka, and E. Gouaux. 2018. Gating mechanisms of acid-sensing ion channels. *Nature*. 555:397–401. <https://doi.org/10.1038/nature25782>
- Zhang, S., J. Arnadottir, C. Keller, G.A. Caldwell, C.A. Yao, and M. Chalfie. 2004. MEC-2 is recruited to the putative mechanosensory complex in *C. elegans* touch receptor neurons through its stomatin-like domain. *Curr. Biol.* 14:1888–1896. <https://doi.org/10.1016/j.cub.2004.10.030>

## Supplemental material

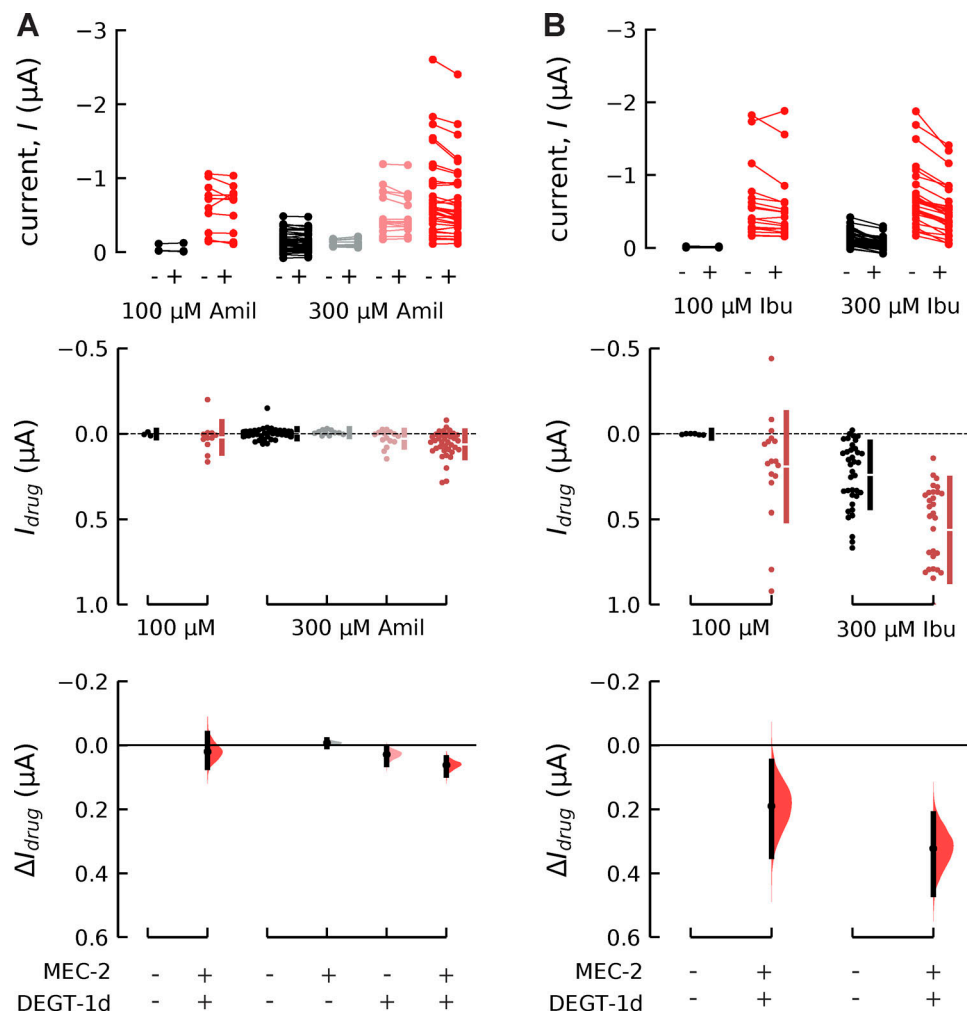


Figure S1. **Sensitivity of DEGT-1d, DEGT-1 alone, and MEC-2 alone to higher concentrations of amiloride and ibuprofen. (A)** Top: Paired dots show the current at  $-85$  mV in uninjected oocytes (black), in oocytes expressing MEC-2 alone (gray), in DEGT-1d alone (light red), and in oocytes coexpressing MEC-2 and DEGT-1d (red) before and after treatment with  $100$   $\mu$ M or  $300$   $\mu$ M amiloride (Amil). Drug-sensitive current ( $I_{drug}$ ; middle) at  $-85$  mV in uninjected oocytes (black), in oocytes expressing MEC-2 alone (gray), in DEGT-1d alone (light red), and in oocytes coexpressing MEC-2 and DEGT-1d (red). Estimation plots (bottom) showing the effect of each drug ( $\Delta I_{drug}$ ) on MEC-2 alone (gray), DEGT-1d alone (light red), and DEGT-1d (together with MEC-2; red) relative to the drug effect on uninjected oocytes. Subsequent estimation statistics are described as a change in current compared with the change in current to uninjected oocytes, the 95% confidence interval (in  $\mu$ A), and the two-sided P value of the Mann–Whitney test:  $100$   $\mu$ M Amil DEGT-1d:  $0.111$   $\mu$ A (– $0.00403$  to  $0.388$ ),  $P = 0.279$  ( $n = 12$ );  $300$   $\mu$ M Amil DEGT-1d:  $0.0623$   $\mu$ A ( $0.0383$ – $0.0922$ );  $300$   $\mu$ M Amil DEGT-1d:  $0.0623$   $\mu$ A ( $0.0383$ – $0.0922$ ),  $P = 1.32e-06$  ( $n = 36$ ); DEGT-1 alone:  $0.0288$   $\mu$ A ( $0.00847$ – $0.0617$ ),  $P = 0.0528$  ( $n = 15$ ); MEC-2 alone:  $-0.0067$   $\mu$ A (– $0.0176$  to  $0.00437$ ),  $P = 0.19$  ( $n = 11$ ). **(B)** Paired dots (top) show the current at  $-85$  mV in uninjected oocytes (black) and in oocytes coexpressing MEC-2 and DEGT-1d (red) before and after treatment with  $100$   $\mu$ M or  $300$   $\mu$ M ibuprofen (Ibu). Drug-sensitive current ( $I_{drug}$ ; middle) at  $-85$  mV in uninjected oocytes (black) and in oocytes coexpressing MEC-2 and DEGT-1d (red). Estimation plots (bottom) showing the effect of each drug ( $\Delta I_{drug}$ ) on DEGT-1d (red) relative to the drug effect on uninjected oocytes. Subsequent estimation statistics are as follows:  $100$   $\mu$ M Ibu DEGT-1d:  $0.19$   $\mu$ A ( $0.0446$ – $0.329$ ),  $P = 0.0229$  ( $n = 17$ );  $300$   $\mu$ M Ibu DEGT-1d:  $0.322$  ( $0.213$ – $0.465$ ),  $P = 2.48e-06$  ( $n = 30$ ).



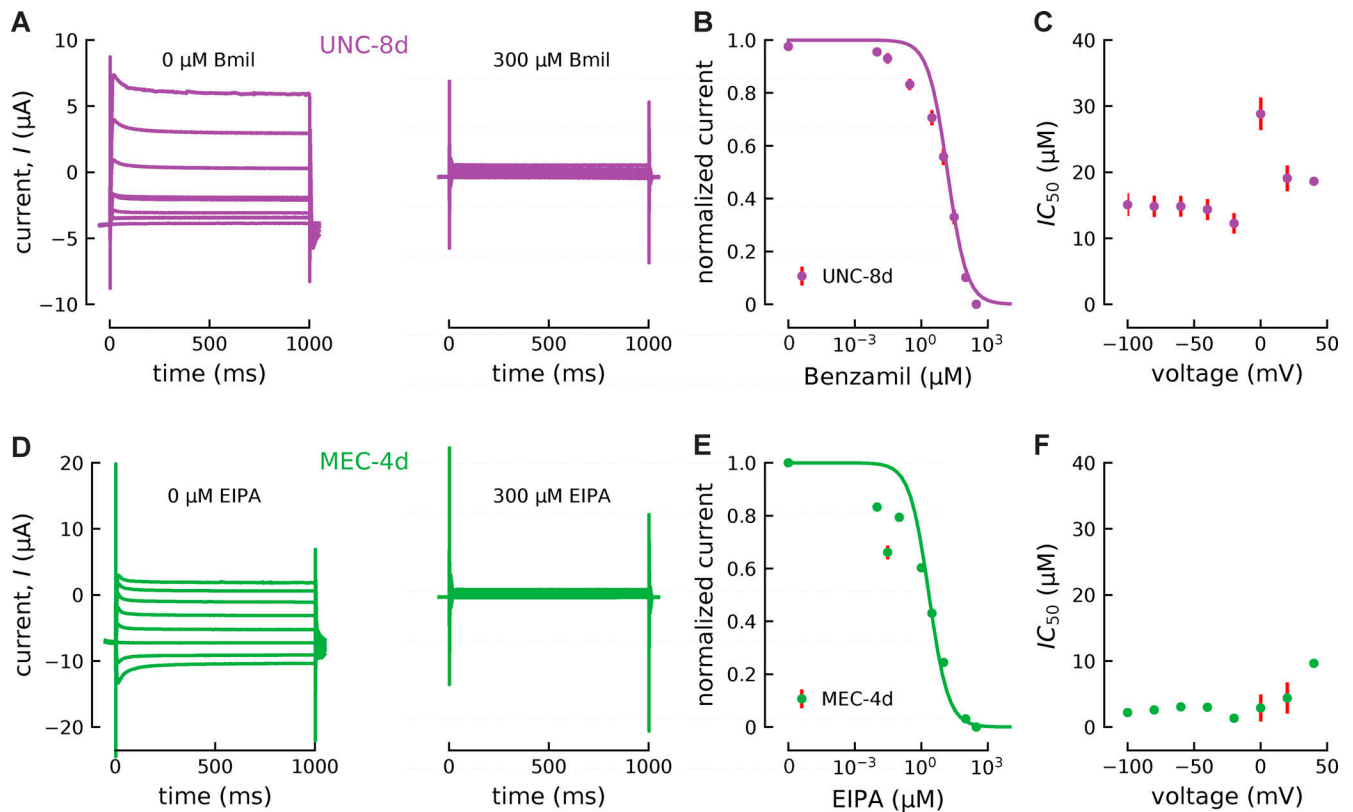


Figure S2. **Sensitivity of UNC-8d channels to benzamil and MEC-4d channels to EIPA.** **(A)** Representative traces of currents of oocytes coexpressing MEC-2 and UNC-8d channels in the absence (left) and presence (right) of 300  $\mu\text{M}$  Benzamil (Bmil). Current responses to voltage steps from  $-100$  mV to  $+40$  mV in 20-mV increments. **(B)** Dose-response curves of UNC-8d channels to Bmil at  $-60$  mV. The mean  $IC_{50} \pm \text{SEM}$  for Bmil at  $-60$  mV was  $14.8 \pm 1.6$   $\mu\text{M}$  ( $n = 4$ ). **(C)**  $IC_{50}$  values for different voltages ( $n = 4$ ). Mean values for dose-response curves were derived from a step protocol similar to Fig. 1 A. Instead of the ramp (red background), voltage steps from  $-100$  mV to  $+40$  mV in 20-mV increments were applied. **(D)** Representative traces of currents of oocytes coexpressing MEC-2 and MEC-4d channels in the absence (left) and presence (right) of 300  $\mu\text{M}$  EIPA. Voltage pulses were applied between  $-100$  and  $40$  mV (20-mV increments) from a holding potential of  $-60$  mV. Similar results were obtained in a total of 11 oocytes isolated from three frogs. **(E)** EIPA dose-response relationship of MEC-4d current at  $-60$  mV (normalized to  $I_{\text{max}}$  and baseline current). Points are the mean  $\pm$  SEM analyzed from at least three donor frogs, and the smooth line is fit to these points using a single-binding site curve. **(F)**  $IC_{50}$  as a function of voltage (points are the mean  $\pm$  SEM,  $n = 11$ , except  $0 + 20$  mV,  $n = 2$ , and  $+40$  mV,  $n = 1$ ). Smooth lines in B and E are fits of the data to the Hill equation (see Materials and methods).